Journal of
Materials Chemistry C

REVIEW

View Article Online
View Journal | View Issue

Cite this: J. Mater. Chem. C, 2018, 6, 11795

Recent developments in photonic, plasmonic and hybrid nanowire waveguides

Sanggon Kim[a] and Ruoxue Yan *[ab]

Received 17th June 2018,
Accepted 25th July 2018

DOI: 10.1039/c8tc02981d

rsc.li/materials-c

Recent years have seen a rapid expansion of research into photonic and plasmonic nanowire waveguides for both fundamental studies and technological applications, because of their ability to propagate and process optical signals in tightly confined light fields with high speed and low power, space and material requirements. This comprehensive review summarizes recent advances in the fabrication, characterization and applications of both photonic and plasmonic NW waveguides, with a special focus on the comparative discussion of their differences and similarities in mechanisms and properties, strengths and limitations in performance, and how they can work together in hybrid devices with performances and applications that neither can achieve individually. We also provide an outlook on the future opportunities and directions in this exciting field.

1. Introduction

Photons, as fundamental carriers of information, outperform electrons in every aspect of long-distance data communication, including transmission speed, bandwidth and energy loss. With the invention of lasers, amplifiers and low-loss optical fibers, photons have taken over the market of long-range data communication that has been ruled by electrons over the last century. Still, the battle between electrons and photons has never stopped and is taking place now at a much smaller length scale. While the microelectronics industry works relentlessly in confining electrons in smaller electronic components for faster signal processing and lower energy consumption, confining

[a] Department of Chemical and Environmental Engineering, University of California, Riverside, USA. E-mail: rxyan@engr.ucr.edu
[b] Materials Science and Engineering Program, University of California, Riverside, USA

Sanggon Kim

Sanggon Kim received his BS in Chemical Engineering in 2009 and MS in Semi-conductor and Chemical Engineering in 2012 from Chonbuk National University, and PhD in Chemical and Environmental Engineering from the University of California, Riverside, in 2018. He worked on the design and synthesis of novel catalysts and nanostructured biosensing materials. Currently, his research is focused on plasmonic nanowire waveguides and their applications in advanced microscopy for nanoscale chemical analysis and imaging.

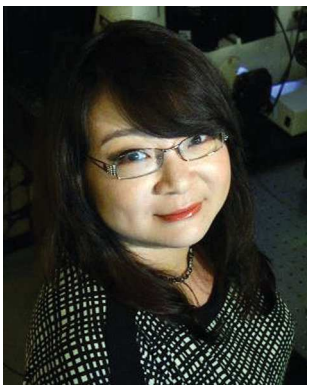

Ruoxue Yan

Professor Ruoxue Yan received her PhD degree in Chemistry from UC Berkeley in 2010 under the supervision of Prof. Peidong Yang, where her research was focused on nanowire photonics and plasmonics. Then she continued to serve as a postdoc researcher in Laurence Berkeley National Lab, where she worked on spectroscopic studies of heterogeneous artificial photosynthesis reactions using nanoplasmonic platforms. She is currently a tenure-track assistant professor at the Department of Chemical and Environmental Engineering, University of California, Riverside, and a recipient of the NSF CAREER Award for the development of advanced chemical imaging spectroscopy using photonic and plasmonic nanowires. Her research is focused on high performance nanomaterials for advanced photonics, electronics, and biological applications.

light in tighter optical cavities is also the holy grail for integrated optical circuits, optoelectronics and nano-sensors for the very same reasons. In this battle at the nanoscale, however, photons are lagging behind despite being the fastest runners of all particles and their broad-band nature in signal propagation. Their wavelengths (λ_p) are orders of magnitude larger than the de Broglie wavelength (λ) of electrons, making it much more difficult to localize photons into nanoscale regions and limiting the level of integration and miniaturization available.

Over the last two decades, nanowires (NWs), which are natural one-dimensional optical waveguides or nanoscale optical fibers, have been intensively studied due to the exquisite synthetic control developed over their dimensions, crystal structures, compositions, and structural/compositional complexity. The unprecedented versatility and tunability of the nanowire platform were testified by the success of an impressive number of waveguide-based sub-wavelength devices, ranging from active optoelectronic devices like lasers/LEDs/photodetectors, to passive waveguides for optical circuit integration, and to a single cell endoscope that is capable of delivering and collecting optical signals to/from subcellular regions.

The real challenge for the nanowire waveguides to rival their electronic counterparts is to achieve a similar level of miniaturization. The smallest cross-sectional size for a dielectric waveguide to support propagating photons is dictated by the Abbe's diffraction limit and is roughly half of the wavelength of the photon in the waveguide.[1] This size limit was shifted to the subwavelength region (down to 100 nm) using single crystalline high refractive index nanowires, *e.g.*, SnO_2 (n = 2.1), with a low propagation loss (1–8 dB mm^{-1}) at visible frequencies.[2] However, further miniaturization of optical waveguides is still hindered by the diffraction limit. To address this challenge, plasmonic or metal nanowires with negative dielectric permittivity were brought to the forefront of nano-waveguide research in the past decade. Plasmonic waveguides transmit electromagnetic energy at optical frequencies with surface plasmon polaritons (SPPs), which travel on metal nanowire surfaces as collective oscillations of free electrons coupled to the electromagnetic wave. The energy is tightly confined at metal surfaces to as small as a few nm and allows for deep subwavelength localization. However, as a trade-off, the propagation losses in metal nanowires, even for the most conductive metal (Ag) on earth, are far larger than those in their dielectric counterparts, arising from the ohmic loss caused by the scattering of oscillating electrons and can reach the level of $\sim$1 db μm^{-3}, 3 orders larger than those in their dielectric counterparts. Accompanying the tight spatial energy confinement on plasmonic nanostructures is the massive enhancement of the local electromagnetic field, which in turn enhances the magnitude of light–matter interactions near the metal surface, enabling high sensitivity chemical and biological sensing and imaging. The distinct characteristics of dielectric and metal NWs dictate the way they are incorporated into different nanophotonic applications (Fig. 1).

There have been a considerable number of review papers that separately covered dielectric[4–7] or metal NW waveguides,[8–10] possibly due to their distinctively different waveguiding mechanisms, synthesis, performance and applications. However, very few focus on the comparative discussion of their differences and similarities in properties, strengths and limitations in performance in the context of different nano-optical applications and how they can work together in hybrid devices with performances and applications that neither can achieve individually. In this review, we will first address the differences in waveguiding mechanisms and the fundamental limits of dielectric and plasmonic waveguides, then review recent advances in the exquisite synthetic control over the size, morphology and composition of optical nanowires to tailor their performance and integrate multiple functions towards specific applications. We will also highlight the remarkable progress in nanoscale optoelectronics and sensing and imaging tools in the last decade enabled by nanowire waveguides and compare the strengths and limitations of dielectric and metallic waveguides in each application. Lastly, we will highlight recent developments of hybrid photonic–plasmonic waveguides, which promise to bring in the best of both worlds: the tight spatial confinement of the plasmonic waveguide and the low propagation loss in the dielectric waveguide.

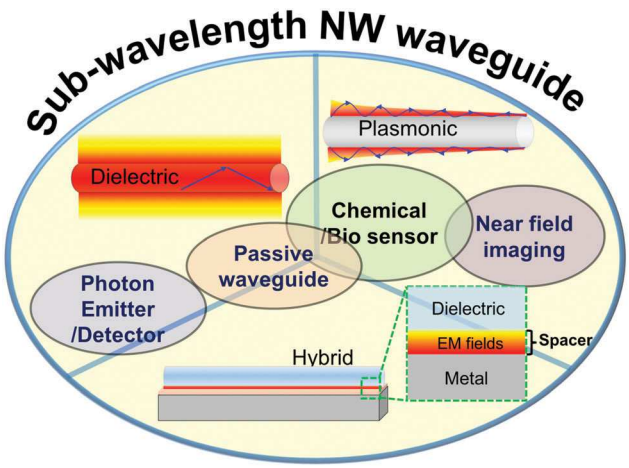

Fig. 1 Classification of sub-wavelength NW waveguides.

2. Light propagation in photonic and plasmonic nanowire waveguides

Both photonic and plasmonic nanowires can function essentially as subwavelength optical waveguides, which transmit optical energy in the form of a wave while confining the energy inside or close to the nanowire. However, the ways in which energy is transmitted in them are completely different, which dictates their distinct optical performances. The rational design of the composition and structure of the subwavelength waveguides and the corresponding nanophotonic devices both rely on the understanding of their fundamental waveguiding mechanism and optical behavior, which will be detailed and compared in this section.

In a photonic waveguide, light is guided by diffraction, or total internal reflection (TIR). When a plane wave passes

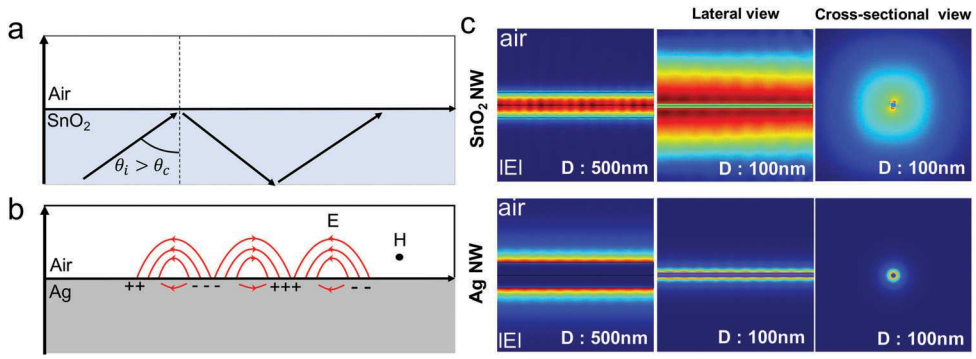

Fig. 2 Comparison of light propagation in dielectric and metallic waveguides. (a) Total internal reflection of wave in the dielectric waveguide. The insets show the electric-field distribution in SnO_2 (b) light propagation as SPP at the interface between metallic and dielectric materials. (c) Electric-field distribution in the SiO_2 and Ag nanowire waveguides with 500 nm diameter and 100 nm diameter. The wavelength of the incident light is 700 nm. θ_i and θ_c are the incident and critical angles of light respectively.

through the boundary of a medium with a high refractive index (n_1), *i.e.*, the waveguide, to the one with a low refractive index (n_2), *i.e.*, the dielectric cladding or in many cases air, total internal reflection occurs when the incident angle is larger than the critical angle $\theta_c = \sin^{-1}\left(\frac{n_2}{n_1}\right)$ (Fig. 2a). When light is coupled at one end of the waveguide, any photon that enters at a wrong angle ($<\theta_c$) leaks out from the waveguide as coupling loss, and those with the right angles ($>\theta_c$) survive and bounce back and forth on the interfaces through TIR, so the electromagnetic energy, or data/information if the light is modulated, can propagate in the waveguide with little energy loss and at the speed of light. A dielectric waveguide is able to carry many independent channels, each using a different wavelength of light, giving it inherently high data-carrying capacity, or bandwidth.

In order to scale down the size of optical components for nanophotonic integration, deep-subwavelength confinement is required, which means a waveguide should be able to confine and propagate light with a wavelength much larger than the cross-section of the waveguide itself. In dielectric waveguides, the level of confinement available is dictated by the diffraction limit, which puts the smallest waveguide diameter at $\sim\lambda/(2n)$, where λ is the wavelength of light in vacuum and n is the refractive index of the waveguide material. By replacing SiO_2 (n = 1.5), the core material in optical fibers, with higher refractive index materials, such as SnO_2 (n = 2.1), the size limit can be pushed to the subwavelength region. Tremendous efforts in nanomaterial synthesis in the past several decades has led to a rich collection of single crystalline high-index dielectric nanowires with atomically smooth side walls, high purity and uniform diameters to ensure low propagation losses even in the subwavelength regime, and impressive tunability in size, shape and composition.[11] However, the wavelength to diameter ratio achievable is still fundamentally limited. This can be understood by comparing the electric field distribution of guided fundamental modes in high index SnO_2 fibers of different diameters (Fig. 1c, top panels). As the fiber diameter, d, decreases from 500 to 100 nm, the fundamental mode (λ = 700 nm) becomes less contained in the fiber and the electromagnetic energy starts to extend deep into the air. Despite the decrease in waveguide size, the size of the guided mode increases significantly beyond the diffraction limit and will eventually become a bulk plane-wave in air, or free-space photons.

The situation for guiding SPP modes in plasmonic waveguides is drastically different. In a metallic waveguide, conduction electrons interact strongly with the incident light, which is essentially oscillating electromagnetic fields, to form polaritons on the metal surface in the form of collective free electron oscillations that can propagate along the waveguide (Fig. 1b). Such a propagating electron density wave is termed surface plasmon polaritons and is free from the spell of the diffraction limit of light. Different from dielectric waveguides, where the energy of guided modes is confined within the waveguide, SPP modes are surface bonded to the metal and their electromagnetic field dampens exponentially into the metal and the surrounding medium. As a result, the electromagnetic fields are tightly confined to the metal waveguide surface. When the diameter of a metal decreases, the size of the fundamental SPP mode shrinks accordingly (Fig. 1c, bottom panel), and can theoretically be compressed down to a few nm.[12]

However, plasmonic waveguides have their own limitations. The energy dissipation of SPPs is orders of magnitude higher than dielectric waveguides, due to an exponential damping term in the wave equation in the propagating direction, which is contributed by the imaginary part of the metal relative permittivity. This energy loss originates from inelastic scatterings of free-electrons during the collective oscillation with the lattice, defects, grain boundaries and surfaces, and is physically the same as the ohmic loss in an electric cable that conducts current from the collective movement of free electrons. And similar to an electrical conductor, where the resistance increases with decreasing cable diameter, the propagation loss in plasmonic waveguides also increases as the waveguide becomes smaller, or in other words, as the mode confinement becomes tighter.[13,14] To compensate for the high loss at the deep-subwavelength dimensions, careful choice of materials and nanowire fabrication methods is extremely important.

That is why, Ag, which is the most conductive of all metals and free of any inter-band transition in the visible-NIR range, is the best choice of material. Chemically synthesized Ag nanowires are preferred over lithographically defined nanowires because they are highly-crystalline with low defect levels and have atomically smooth surfaces that work together to minimize the propagation loss. Nevertheless, the capability of plasmonic nanostructures to achieve deep-subwavelength localization of the guided signals brings them to the forefront of the research towards highly integrated nano-optic circuits and components, as well as the delivery of light to the nanoscale.

3. Synthesis of photonic and plasmonic nanowire waveguides

Over the last decade, the general strategies for optical nanowire synthesis and fabrication have not changed substantially. Rather, world-wide research effort has been devoted to precisely controlling the nanowire dimensions, compositions, defects and crystal structures, aiming towards optimizing their optical performance, and to rationally integrating different functionalities through longitudinal and lateral heterostructures. In this section, we review important new advances in the synthesis of both photonic and plasmonic nanowire waveguides with a focus on ''bottom-up'' chemical synthesis. This is because chemically synthesized nanowire waveguides, especially at the subwavelength dimensions, outperform those fabricated by almost any ''top-down'' lithographical methods in terms of sidewall smoothness, diameter uniformity, compositional purity and crystalline quality, which work together to minimize propagation losses. Furthermore, different optical properties can be incorporated within a single NW by actively manipulating synthesis parameters to tune its composition and structure during growth, which opens up new avenues for highly integrated single nanowire photonics.

3.1. Gas phase synthesis technique

As stated above, the creation of nanowires for subwavelength photonics is heavily dependent on the controlled synthesis of high quality one-dimensional materials. Until now, an impressive number of methods have been developed to serve this purpose: CVD, CVT, molecular beam epitaxy, vapor–solid–solid, vapor–solid, oxide-assisted growth, templated growth, solution–liquid–solid growth, supercritical fluid liquid solid growth, solvothermal/hydrothermal synthesis, directed solution phase growth, *etc.*[15] Among them, gas phase synthesis, vapor–liquid–solid (VLS) growth in particular, is the most widely adopted growth technique for high-quality photonic nanowires due to its flexibility and versatility. By rapidly adsorbing gas phase reactants to the supersaturation level, catalytic liquid alloy droplets on a growth substrate aid the seeded and oriented growth of nanowires, the diameter of which is determined by the catalyst droplet size. Therefore, it has a better capability of controlling the nanowire diameter compared to the catalyst-free methods. The optimum catalyst for a liquid eutectic alloy for the nanowire of interest can be chosen on the basis of the phase diagram. Since its introduction in the early 1960s,[16] this approach has been applied for the synthesis of other semiconductor NWs such as Si[17] and Ge,[18] group III–V (GaAs, GaP, InAs, InP, GaAsP, InAsP), II–VI (ZnS, ZnSe, CdS, CdSe), and IV–VI (PbTe).[15,19] However, one inherent problem of VLS growth is the diffusion of the metal catalyst into the NW, resulting in charge carrier recombination centers or electron/photon scattering centers,[15,20] which is especially harmful for semiconductor nanowire-based active waveguides. In addition, the chemical removal process of metallic catalysts after growth could impair the optical properties of the NW. Therefore, other catalyst-free synthesis techniques have been studied intensively such as vapor–solid growth, oxide-assisted growth, and templated growth although they are not as popularly used as VLS. In Table 1, where we index the optical properties, synthesis methods, and physical dimensions that can be achieved and applications of major photonic nanowire waveguides, one can find the gas phase synthesis methods adopted for each individual material and the size range available.

Recently, exciting progress in gas phase synthesis was made on improving the optical quality of photonic nanowires derived from these existing growth strategies. The ability to maintain lower defect levels and uniform diameters throughout a significant length required for light propagation pushes the nanowire waveguide one more step towards practical applications. In 2010, Ramdani *et al.* reported the growth of exceptionally long GaAs NWs using Au-assisted VLS-hydride vapor phase epitaxy (HVPE), using gaseous GaCl molecules as the Ga precursor.[21] The dechlorination rate of GaCl is so high that there is no kinetic delay and equilibrium conditions can be quickly established.[22] As a result, less tapered and low defect nanowires can grow at a fast rate of 170 $\mu m\ h^{-1}$ on average. Using a similar strategy, ultralong (130 $\mu m\ h^{-1}$) and defect-free GaN nanowires were also synthesized using HVPE with a broad range of diameters (70–200 nm),[23] as shown in Fig. 3a.

Another example is the growth of stacking-fault-free wurtzite InP NWs by selective-area (SA) metal–organic vapor phase epitaxy (MOVPE).[24] SA-MOVPE has a unique advantage over VLS because it can maintain a much lower impurity concentration by removing metal catalysts, which diffuse into the nanowire at the high growth temperature, creating defects. A uniform diameter distribution along the nanowire was also achieved over a wide size range (80–600 nm) (Fig. 3b). The uniform diameter is important not only for passive waveguiding, but also for improving the optical quality of the Fabry–Perot cavity for low-threshold lasing.

Besides the improvement in nanowire quality, there have also been significant efforts in fine-tuning and rationally controlling the composition within a single nanowire for function integration. In 2011, Yang *et al.* introduced a substrate moving growth strategy for full-color bandgap graded nanowires[25] (Fig. 3c). By controlling the location and moving speed of the substrate during growth, the compositional gradient along a single nanowire was achieved with potential applications in broadband light absorption and emission devices. Discretization of the

Table 1 Homogeneous photonic nanowires for optoelectronics (UV-Visible-NIR)

Materials	Bandgap (eV)	Refractive index (visible to NIR)	Vapor phase		Solution phase		Applications
			Synthesis method	Properties	Synthesis method	Properties	
ZnS	3.7	2.6–2.3	VLS,[50] VS,[51] PVD,[52] MOCVD[51]	*D*: a few ~60 nm *L*: >10 μm	HT/ST,[53] SLS,[51] ECD[54,55]	*D*: a few ~ 15 nm *L*: >1 μm	Emitter/detector (UV)
SnO_2	3.6	2.1–2.0	VLS,[56] VS,[57] PVD[58]	*D*: 30–500 nm *L*: ~a few millimeter	HT/ST[59]	*D*: a few ~100 nm *L*: ~100 μm	Waveguide
GaN	3.4	2.6–2.3	VLS,[60] VS,[60] PVD,[61] MOCVD[62]	*D*: a few ~100 nm *L*: >10 μm	N/A	N/A	Emitter/detector (UV), Waveguide
ZnO	3.37	2.1–1.7	VLS,[63] VS,[60] PVD,[64] MOCVD[65]	*D*: a few ~300 nm *L*: ~ a few millimeter	HT/ST,[66] ECD,[67] Sol–gel[68]	*D*: 10–300 nm *L*: ~10 μm	Emitter/detector (UV), Waveguide
TiO_2	3.2	3.3–2.7	VLS,[69] PVD[70]	*D*: a few~ 500 nm *L*: ~10 μm	HT/ST,[71] ECD,[72] Sol–gel[73]	*D*: 10–100 nm *L*: >10 μm	Waveguide
ZnSe	2.7	2.9–2.4	VLS,[60] PVD,[74] MOCVD[75]	*D*: a few~ 80 nm *L*: ~10 μm	SLS,[76] ECD[77]	*D*: 10–40 nm *L*: >10 μm	Emitter/detector (Visible)
CdS	2.42	2.1–1.7	VLS,[60] VS,[78] PVD,[79] MOCVD[80]	*D*: a few ~500 nm VLS *L*: ~100 μm	HT/ST,[60] SLS,[81] ECD[82]	*D*: 10–100 nm *L*: >10 μm	Emitter/detector (Visible)
GaP	2.26	4.2–3.1	VLS[60]	*D*: a few ~30 nm *L*: >10 μm	SLS[60]	*D*: 10–30 nm *L*: ~10 μm	Emitter/detector (Visible)
ZnTe	2.26	2.7–3.7	VLS[83]	*D*: a few ~200 nm *L*: >20 μm	SLS,[84] HT/ST[85]	*D*: 40–60 nm *L*: >45 μm	Emitter/detector (Visible)
CdSe	1.74	2.7–2.4	VLS[60]	*D*: a few~ 30 nm *L*: ~10 μm	SLS,[60] ECD[86]	*D*: a few ~33 nm *L*: >10 μm	Emitter/detector (Visible)
CdTe	1.5	3.7–2.6	VLS,[87] MOCVD[88]	*D*: a few ~100 nm *L*: ~100 μm	SLS,[60] ECD,[89] HT/ST[90,91]	*D*: a few ~10 nm *L*: >10 μm	Emitter/detector (NIR)
GaAs	1.42	5.1–3.3	VLS,[60] VS,[60] MOCVD[92]	*D*: a few~200 nm *L*: >10 μm	SLS[84]	*D*: a few ~40 nm *L*: ~10 μm	Emitter/detector (NIR)
InP	1.344	4.4–3.1	VLS[60]	*D*: a few~ 30 nm *L*: ~10 μm	SLS[60]	*D*: a few ~20 nm *L*: >10 μm	Emitter/detector (NIR)
Si	1.1	5.6–3.4	VLS,[60,93] VS[94]	*D*: a few ~20 nm *L*: ~30 μm	SLS,[95] ECD[96]	*D*: a few ~50 nm *L*: >20 μm	Emitter/detector (NIR), Waveguide
GaSb	0.726	5.2–3.8	VLS,[97] VS,[98] MOCVD[99]	*D*: ~30 nm *L*: >10 μm	N/A	N/A	Emitter/detector (NIR)

VLS: vapor–liquid–solid, VS: vapor–solid, SLS: solution–liquid–solid, HT/ST: hydrothermal/solvothermal, ECD: electrochemical deposition, PVD: physical vapor deposition, MOCVD: metallic–organic chemical vapor deposition.

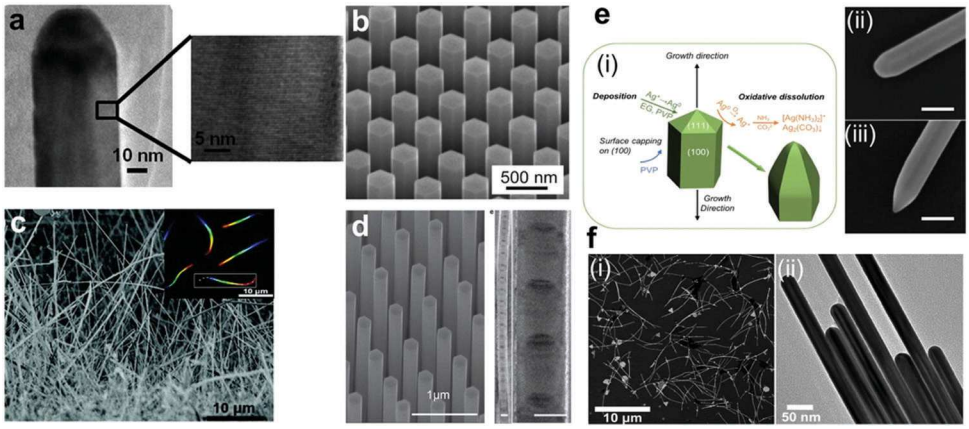

Fig. 3 Recent advances in the gas and solution phase-based synthesis of nanowire waveguides. (a) TEM images of GaN nanowires grown by hydride vapor phase epitaxy (HVPE) with a fast growth rate and high crystalline quality or low impurities. Adapted with permission from ref. 23. Copyright 2014 American Chemical Society. (b) SEM image of periodically aligned InP nanowire arrays grown with selective-area metal–organic vapor-phase epitaxy (MOVPE or MOCVD). Adapted with permission from ref. 24. Copyright 2014 American Chemical Society. (c) SEM images of band gap graded full-color nanowires. The top inset shows the real photograph of the full-composition AnCdSSe nanowires under the illumination of a 405 nm laser. Adapted with permission from ref. 25. Copyright 2011 American Chemical Society. (d) SEM and STEM image of a stacked $In_{0.22}Ga_{0.78}As$/GaAs quantum dot embedded nanowire. Scale bar, 50 nm. Adapted with permission from ref. 26. Copyright 2015 Springer Nature. (e) Schematic of the dynamic control of the deposition and dissolution rates at the tip of the AgNW. SEM images of AgNW tips sharpened with oxidative dissolution of the silver at the tip of the nanowire. Scale bar, 100 nm. Adapted with permission from ref. 27. Copyright 2016 American Chemical Society. (f) SEM (i) and TEM (ii) images of highly crystallized Au nanowires synthesized by a room temperature acidic solution route with diameter and length tunability. Adapted with permission from ref. 28. Copyright 2008 American Chemical Society.

bandgap even further using quantum confined structures as an active medium in a passive nanowire waveguide is another approach for functional integration on a single wire level.[29–32] The incorporation of densely-packed, strain-relieved quantum dots (QDs), which have discretized density-of-states (DOSs) induced by quantum confinement, into the nanowire cavity is expected to offer a dramatic improvement in lasing performance. In 2015, Tatebayashi *et al.* experimentally demonstrated room-temperature lasing for the first time in multi-stacked $In_{0.22}Ga_{0.78}As$ QDs in a single GaAs NW capped with an AlGaAs/GaAs shell for passivation.[26] The site-controlled growth is achieved by lateral-flow, low-pressure selective metalorganic chemical vapor deposition (MOCVD) with a modulated mixing ratio of the group III precursors. The use of $In_{0.22}Ga_{0.89}As$ QDs instead of InAs[33] leads to the reduction of accumulative compressive strain to achieve strain-relieved growth. This level of structural and compositional complexity requires careful design of the growth parameters based on a diffusion–deposition model of the morphological evolution of nanowires and property optimization based on optical characterization combined with numerical analysis.

3.2. Solution phase synthesis technique

Solution phase synthesis for dielectric/semiconducting nanowires, including solvo/hydrothermal, Solution–Liquid–Solid (SLS), hot-injection, soft and hard templating methods, is considered the most attractive synthesis route for the large-scale production of nanowires, because of its simplicity, versatility, low energy consumption, fast growth, and in many cases, its environmental friendliness. It is obvious from Table 1 that all major photonic nanowires were successfully fabricated using solution-based methods. However, because of the relatively low growth temperature and, in many cases, the use of shape-directing molecules and ions, solution phase methods tend to yield nanowires with higher trap-site defect levels compared to vapor-phase growth. The photoluminescent quantum efficiencies (QEs) reported for ensembles of colloidal semiconductor nanowires were around 0.1–0.3%.[34–37] This has put the colloidal photonic nanowires at a disadvantage for optoelectronic applications, where extremely high material quality is required to achieve high-efficiency. It should be noted that quantum nanowires with high photoluminescence efficiencies[38] were successfully demonstrated through the TOPO based hot injection method, although the diameters are much beyond the diffraction limit for waveguide-based applications.

The solution-phase growth of common plasmonic nanowires is a completely different landscape. Synthesis of plasmonic NWs was predominantly achieved in solution at a relatively low temperature ($<200\ ^{\circ}C$) through simple reduction-precipitation reactions. Here we focus on Ag and Au nanowires because they are the most commonly investigated for waveguiding, due to their relatively low optical loss in the visible and NIR spectral range. Both Au and Ag are face-centered cubic crystal structures, which are inherently homogeneous. To aid the one-dimensional growth, capping agents need to be introduced to change the free energies of crystallographic surfaces and change their respective growth rate. High-quality, uniform silver NWs have been synthesized using polyol methods developed by the Xia group in 2002,[39,40] where Ag ions supplied by $AgNO_3$ was reduced by ethylene glycol, which is also the solvent, in the presence of a shape-directing capping agent (polyvinylpyrrolidone, PVP) and complexing ions

(halide ions) to control the growth speed. These NWs have high-crystallinity, low impurity level and atomically smooth surfaces, which work synergistically to make these nanowires the lowest loss plasmonic nanowaveguide. This highly reliable and reproducible method has since then been widely adopted for both research-oriented and commercial production of Ag NWs, with various minor modifications.

Only until very recently was this synthesis revisited to gain the ability to fine-tune the tip geometry of the AgNWs, motivated by the possibility of using AgNWs for high-resolution scanning probes for simultaneous morphological and optical imaging. To gain the nanoscale resolution, the naturally pyramidal or rounded tips must be further sharpened to reduce tip radii. Our group has recently demonstrated that by accelerating the oxidative etching, sharp-tip AgNWs can be synthesized with high uniformity with a diameter of 70 ± 7 nm and an average tip radius of 9 ± 5 nm.[27] These sharp-tip AgNWs have demonstrated 6 nm spatial resolution in morphological imaging, which paves the way to high-resolution near-field optical imaging and sensing, where the spatial resolution depends on how tightly electromagnetic fields can be confined at the tip apex, and scale with the tip curvature.

While many studies have been reported on Ag NW synthesis, only a few have been reported for Au NW synthesis,[41–44] especially with suitable diameters, lengths, crystalline quality and sidewall smoothness for waveguides, and the strategies for size, morphology and structure control have not been developed as comprehensively as for Ag. However, we noticed a recent report on a room temperature synthesis method[28] that yields crystalline, high aspect ratio (>200) AuNWs with atomically smooth sidewalls and diameters suitable for plasmonic waveguides. This is achieved by carefully controlling the seed concentration and lowering the reduction rate in acidic solutions to facilitate the growth of nanowires instead of particles.

4. Applications of photonic NW waveguides

Photonic waveguides have found a wide variety of applications in nanoscale optoelectronics, integrated optical circuits and nanosensing, due to their low propagation loss and high thermal and chemical stability. Semiconductor nanowires are particularly versatile because they have high refractive indices ($n > 2 > n_{SiO_2}$), and generally, show dielectric optical properties and act as passive subwavelength waveguides at frequencies below their band gap. However, when the frequency of light or electrical bias is higher than the bandgap, they act as light emitters or detectors. We want to point out here that tight light confinement is important not only for passive wave guidance in the subwavelength regime but also for integrated optoelectronic devices relying on active light–matter interactions. For example, nanowire lasers are essentially waveguide lasers, and the nanowire doubles as the gain medium and a Fabry–Perot lasing cavity. Therefore, the ability to tightly confine optical energy is crucial for achieving a high quality factor and low lasing threshold.[6,15,45]

Table 1 summarizes the optical properties and applications in optoelectronics, alongside their common fabrication methods. Many earlier important works in this field have been reviewed extensively, therefore, in this section, we will primarily focus on recent milestones of photonic NW waveguides in different photonic applications.

4.1. Optoelectronics

Bringing the success of photonic waveguide in long-distance data communication to the nanoscale is fundamentally challenging. Despite the efforts in nanophotonics in the past few decades, there still exist many obstacles in realizing a highly-integrated all-optical circuit, especially for complex devices like processors and memory chips. Therefore, the main application of the photonic NW waveguide in optoelectronics is to replace copper wires for the board-to-board, chip-to-chip and intra-chip level data communications, especially in computer data centers, as big data and cloud computing continue to grow exponentially.[46] High volume of data traffic is limited by the bandwidth and microwave losses of copper cables and transmission lines and requires fundamentally higher data transmission density at a small footprint. Further improvement of data transfer speed in copper wires is currently limited by its frequency (<100 MHz), which is proportional to the impedance of the copper lines, while the photon has a much higher frequency ranging from 150–800 THz for the visible and near-infrared spectrum.[8]

The optical components necessary for the integration with signal-processing electronics include light emitters (laser/LED), pathways (passive waveguides) and detectors (photodiodes) with requirements including broad bandwidth, high frequency, high stability, low attenuation and heat generation, low skew, immunity of the signal path to electromagnetic interference, and above all, a small footprint.[47] A smaller device footprint results in lower power consumption, denser interconnects, less sensitivity to propagation loss, easier control of temperature, and lower fabrication cost. The semiconductor NW (III–V, II–VI, or IV–VI) generally satisfies these requirements (Table 1) except for the practical size achievable, due to the diffraction limit and bending loss.

Another family of emerging materials for photonic waveguides is rare-earth based upconversion nanowires. Working on a completely different mechanism than semiconductors, these upconversion nanowire waveguides, formulated by embedding lanthanide ions within an insulating host lattice, have unique advantages inherent to f–f transitions, such as NIR-excitation, narrow linewidth multiband emissions, long lifetime, color-tunability and high photo-stability.[48,49] Although currently limited in the conversion efficiency, NIR-excited upconverison nanowire waveguides signify a wide range of potential applications, particularly in biological sensing and imaging in physiological environments.

4.1.1. Active/functional waveguide: light emitters. The NW that emits or absorbs light is called an active or functional waveguide and the corresponding optoelectronic devices are light emitters (lasers and LEDs) and photodetectors, respectively.

This section will focus on the discussion of nanowire lasers and LEDs.

Following the first demonstration of the ZnO nanowire UV laser in 2001,[45] optically pumped coherent laser emission has been achieved for the entire UV to NIR spectra from a number of different semiconductor nanowires.[6,100–104] These nanowires double as the gain medium and Febry–Perot waveguide cavities to achieve light amplification. In these cavities, the large refractive index difference between the semiconductor material and its surrounding dielectric environment tightly confine emitted light within the nanowire, which results in a large overlap between the guided mode and the semiconductor gain media to build up sufficient resonant feedback. As a result, a high optical gain and quality factor can be obtained.[105] However, further minimization of the nanowire lasers to the deep-subwavelength region is prohibited by increasingly large scattering loss, again dictated by the diffraction limit. In addition, these nanowire cavities generally have low reflectivity at the end-facets, which induces considerable losses and limits the optical gain.[106,107]

Another consideration is how to achieve single mode lasing at room temperature. This is important because a highly resolved frequency mode is necessary to prevent lower data transmission rate and false signaling caused by group-velocity dispersion.[108,109] Typically, a nanowire emits single mode light when its diameter satisfies $1 \approx \frac{\pi D}{\lambda}\sqrt{(n_{\mathrm{NW}}{}^2 - n_{\mathrm{air}}{}^2)} < 2.4$, and the ends are cleaved with the NW length that satisfy the Fabry–Perot optical cavity, $L = m\left(\frac{\lambda}{2n_{\mathrm{NW}}}\right)$, where D is the diameter of the NW, λ is the wavelength of light, n_{NW} and n_{air} are refractive indices of the NW and air respectively, L is the length of the NW, and m is an integer. Because the band structure of semiconductors relies on temperature, multi-frequency modes are easily excited at room temperature unless the lasing cavity becomes much shorter.[102]

However, the shortened cavity path results in a lower optical gain and therefore a higher threshold. To solve this dilemma, Y. Xiao *et al.* demonstrated, in 2011, single mode excitation from a nanowire by manually folding the nanowire with a fiber probe to form loop mirrors.[110] As shown in Fig. 4a–f, the higher reflectivity of the loop mirror enables lasing at a low threshold. However, it is difficult to achieve repeatable and reliable results with fiber probe manipulation, even with the same folding conditions. In 2013, H. Gao *et al.* proposed a cleaved coupled nanowire laser realized by cutting the GaN nanowire using focused ion beam milling (Fig. 4g).[109] Compared to individual nanowires, in the cleaved coupled nanowire with nm gap widths, summation of both the NW lengths provides the gain of the laser while the gap distance narrows the optical band (Fig. 4h–i). This approach is significantly more reliable in achieving single mode selection with a lower threshold.[111]

Recent progress in the synthetic control of the nanowire structure, morphology and composition has led to new possibilities for enhancing the optical performance of nanowire lasers. Recently, a room-temperature lasing threshold of 170 μJ per cm^2 per pulse was reported with stacking-fault-free and taper-free wurtzite InP nanowires (Fig. 5a), which, as we discussed earlier in Section 2 (Fig. 3b), were synthesized with

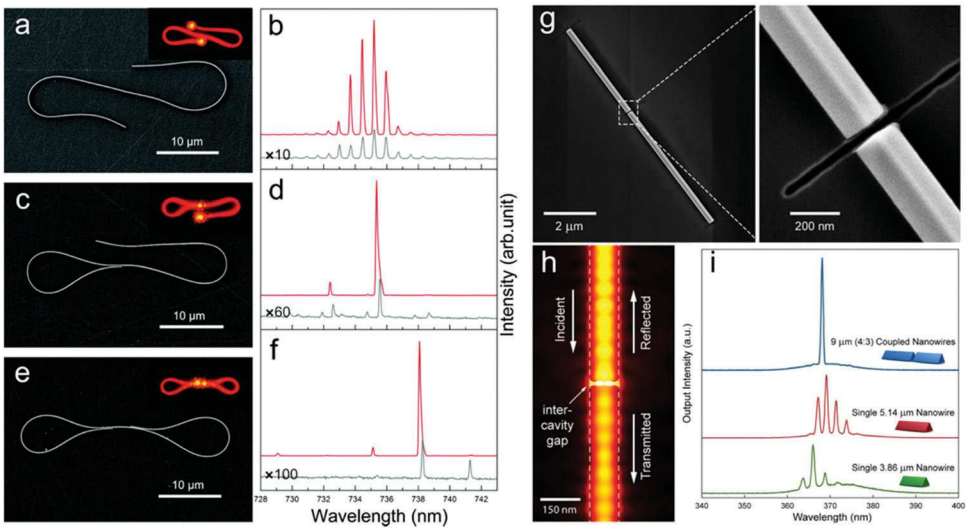

Fig. 4 Mode selection of laser from a single nanowire by nanowire structural change. (a–f) Single frequency laser from a folded single CdSe nanowire. The folded one or two NW ends create loop mirrors (LMs) and coupled resonant cavities. Scanning electron microscopy (SEM) images and lasing spectra of single NW without LM (a and b) and with one LM (c and d), and double LMs (e and f). The insets in the SEM images (a, c, and e) are PL microscopy images. The two spectra with different colors (red and black) were measured with pump fluence far above the threshold and near the threshold respectively. Adapted with permission from ref. 110. Copyright 2011 American Chemical Society. (g–i) Single frequency laser from cleaved-coupled nanowires. (g) SEM images of cleaved GaN nanowires with ~40 nm intercavity gap distance. (h) Simulated electric fields in the NWs near the 20 nm gap width. (i) Photoluminescence spectra of lasing from the individual NW cavity (red and green) and the coupled NW cavity (blue). Single frequency mode was observed with the axially coupled NW cavity, while multiple frequency modes were observed with the individual NW cavities. Adapted with permission from ref. 109.

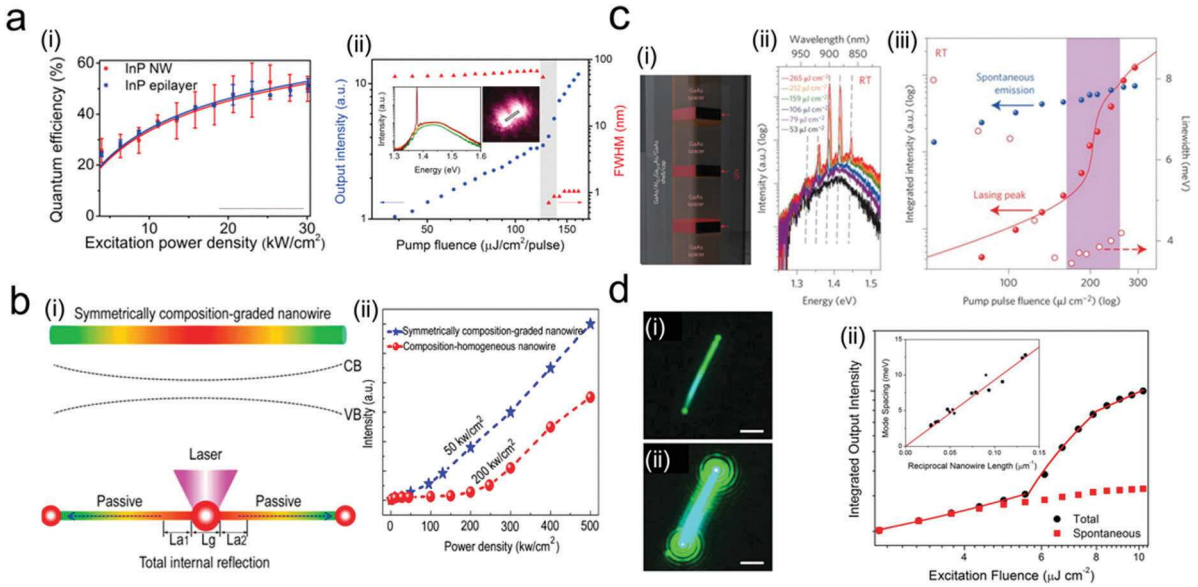

Fig. 5 Enhanced performance in a nanowire emitter and detector through rational synthetic control of structure and composition. (a-i) Comparison of the quantum efficiency of stacking-fault-free and taper-free wurtzite InP nanowires with that of the InP epilayer at room temperature. (a-ii) Emission intensity from a single InP NW showing the lasing threshold in grey where the dramatic reduction of the fwhm of the NW emission spectrum is observed. The inset shows the emission spectra that were obtained at the excitation power densities (110, 130, and 150 μJ per cm^2 per pulse). The optical microscopy image in the right inset shows the NW emission above the threshold. Adapted with permission from ref. 24. Copyright 2014 American Chemical Society. (b-i) Schematic illustration of a symmetrically composition-graded NW with its graded bandgap structure along the longitudinal axis of the NW and the schematic diagram of local excitation at the center of the NW and passive guidance of the excited light to both ends *via* total internal reflection. (b-ii) Comparison of the emission intensity of the symmetrically composition-graded NW with that of a CdS_xSe_{1-x} NW with homogeneous composition as a function of pumping power. Adapted with permission from ref. 112. Copyright 2013 American Chemical Society. (c-i) Schematic illustration of GaAs/$Al_{0.1}Ga_{0.9}As$/GaAs core–shell nanowires with stacked $In_{0.22}Ga_{0.78}As$/GaAs quantum dots. Emission spectra (c-ii) and intensity (c-iii) at various pump pulse fluences showing 179 μJ cm^{-2} threshold of the GaAs nanowires with quantum dots. Adapted with permission from ref. 26. Copyright 2015 Springer Nature. (d-i) Lasing in $CsPbBr_3$ nanowires excited from a femtosecond pulsed laser with two different pump powers. (d-ii) Integrated output intensity of the $CsPbBr_3$ nanowires as a function of pump fluence that shows 5 μJ cm^{-2}. Adapted with permission from ref. 6.

catalyst-free SA-MOVPE.[24] The low-defect density and uniform lateral dimensions contributed to the high optical gain and quality factor of the Fabry–Perot cavity. Guo *et al.* demonstrated another concept for reducing the lasing threshold using a symmetrically composition-graded CdS_xSe_{1-x} NW[112] (Fig. 5b(i)). The composition of the NW is symmetrically changed from the center to both ends. This symmetrical composition gradient reduces the propagation loss of the guided light due to the gradually broadened band gap toward both ends where the excited light is passively guided. Fig. 5b(ii) shows that the lasing threshold was reduced by a quarter compared to a compositional homogeneous nanowire waveguide. The incorporation of lower-dimensional quantum nanostructures into the nanowire is expected to significantly improve laser performance, including the lasing threshold, differential gain, modulation bandwidth and temperature sensitivity, due to the discretized density-of-states induced by quantum confinement. As discussed earlier in Section 2, Tatebayashi *et al.* reported the first single NW laser with homogeneously-stacked $In_{0.22}Ga_{0.78}As$ QDs in a single GaAs NW capped with an AlGaAs/GaAs passivation shell[26] (Fig. 5c(i)). The incorporation of QDs into the nanowire has led to a room-temperature lasing threshold of 179 μJ cm^{-2} per pulse at 1.38 eV, marking a major step towards the future realization of high-performance, low power consumption, ultrasmall nanowire lasers *via* suitable bandstructure/strain engineering.

It is also worth noting that the discovery of new optical materials has also brought new opportunities into nanowire lasing. $CsPbBr_3$ perovskite nanowires synthesized using a solution phase reaction at low temperature have demonstrated a substantially low lasing threshold of 5 μJ cm^{-2} (Fig. 5d). The perovskite nanowire is single crystalline with well-formed facets for optical resonance with a quality factor of ~1000 and high chemical stability under operation conditions, and the emission wavelength is tunable by substituting the halide.[6,104,113]

Electrically driven light emission from NWs is uniquely attractive, mainly because their easy on-chip integration with electronic information processing devices, and smaller footprint and lower energy consumption. Light emitting diodes (LEDs) emit light at band-gap wavelength through the recombination of the electrons and holes separated by electrical energy. In early reports, NW LEDs were realized by combining deposited p-type planar substrates with n-type NWs directly grown on them. A large variation of the turn-on voltage was inevitable due to the poor hole mobility of the planar substrate contributed by the low crystallinity.[102,114] Afterward, the NW LED was realized by crossing single crystal p and n-type NWs with high electron and hole mobility.[115] Interestingly, the electroluminescence excited at the cross junction can be coupled in and guided through the n-type waveguide with a forward bias. However, the asymmetric point at the junction

between the two NWs still can act as a scattering spot leading to an inefficient optical cavity and therefore poor spectral resolution. Later on, an electrically driven single photon source was firstly demonstrated with an axial hetero-structure NW using GaAs/GaP and n-InP/p-InP.[31] The emission efficiency could have been improved by radial hetero-structure NWs due to a larger area for carrier injection or collection. The introduction of a multi-quantum well in the NW with a tunable band gap enables an efficient radiative recombination and control of the wavelength spectrum.[116]

4.1.2. Active/functional waveguide: photodetectors. Another important component for integrated optoelectronics is nanostructures that efficiently detect optical inputs and process them as electrical outputs. The nanowire is uniquely suited for such devices because of their efficient optical absorption and high photocarrier collection efficacy.[117–120] Early work on nanowire photodetectors used a horizontal transistor, which can be turned from an insulating to a conducting state by an optical gate.[121–123] Commercialization of nanowire photodetectors relies on achieving higher photoresponsivity at the nanoscale with a fast response. One way to boost photoresponsivity and quantum efficiency is to reduce the carrier diffusion length by using core–shell heterostructure NWs, where current is collected laterally instead of at the ends of the nanowire. By shortening the carrier diffusion length by a couple of orders of magnitude, detrimental carrier recombination is effectively avoided.[124,125] Practical application of nanoscale photodetectors also demands room-temperature operation, which places even more stringent requirements on device performance, because the sensitivity of the detector is critically influenced by thermally generated carriers.[126] Recently, broadband room-temperature photodetection from 632 nm to 1.5 μm was demonstrated in single InAs NW based Schottky–Ohmic contacted photodetectors.[127] Other III–V semiconductor NWs operated at room temperature such as GaAsSb and hetero-junction GaSb/GaInSb NWs have been reported for NIR photodetection.[127–130] In addition, quantum well, disk, and dot embedded NWs[131] and perovskite NWs[132] akin to the NW lasers and metal–semiconductor–metal radial architecture nanowires[133] (hybrid mode waveguide) have been developed to improve the photoresponsivity and tunability. Details of the hybrid devices will be discussed in the following hybrid waveguide section.

4.1.3. Passive waveguides. The data transmission rate for short distance communication, such as integrated circuits on a board or intra-chip interconnects, is also significantly limited by the bandwidth of the passive waveguide because the long-distance travel of the light occurs mainly here.[134,135] For passive waveguides at the subwavelength scale, the primary design consideration is to maintain guided modes with a low propagation loss. Surface roughness, high refractive index contrast, and randomly distributed scattering centers (impurity atoms, lattice defects, *etc.*) are the main reasons for the propagation losses in dielectric NWs, whereas absorption near the band edge is also a considerable source of loss in the semiconductor.[136] Many of these problems are rooted in the microstructure of the material, which can be controlled in the growth process. Besides the loss from intrinsic material properties, the main loss which occurs during the integration of the NWs into the optical circuits is bend loss. Compact packaging of the waveguides on a small footprint can result in a considerable bending loss. The bending losses depend on the refractive index difference between the NW and the dielectric medium surrounding it, NW diameters, and the wavelength of light, which work together to determine the number and weight of modes in the NW waveguide.[137,138] At the sub-wavelength scale, the fundamental mode, which has no cut-off diameter, is the one guided mode that can be supported and has a large evanescence field outside of the waveguide. In this case, the waveguide packaging for intra-chip communication must be carefully designed because the mode fields in the waveguide can be easily lost by a slight bend.

There are various NWs suitable for a passive waveguide of optoelectronic technology (Table 1). It is worth mentioning that, although outside of the realm of chemically synthesized NWs, the lithographically defined SiO_2 or Si NW has a unique advantage due to the prospect of monolithic integration with signal-processing electronics on a single silicon chip. Enhancement of the mode confinement by increasing the refractive index of silica (1.45) has been achieved by introducing impurities with a higher index, such as SiN.[139,140] However, the major concern with the SiO_2 or Si waveguide was the scattering loss introduced by the top and sidewall roughness ($\sim$1 dB cm^{-1}).[141,142] In contrast, geometric or structural scattering can be negligible for the NW waveguide grown using high-temperature gas phase techniques. This, combined with the large selection of high-index NWs, gives chemically grown NWs a special edge in performance and offers new design-by-choice schemes.[2,4,134]

4.1.4. Integration of active and passive waveguide. To realize on-chip light signal processing, it is ideal to integrate the three waveguide components (light generation, propagation and detection) into a single NW or at least through low-loss optical coupling of different single-wire devices. The coupling of photonic modes between different nanowire waveguides through the evanescent field, or the ''dark mode'', is favored, because this configuration does not require free space light coupling which has a large scattering loss and low coupling efficiency. It also reduces the transition time and fabrication cost and maintains the overall device foot-print low, and more robust against external mechanical impacts. Considerably high light coupling from the active to the passive waveguide with a parallelly aligned NW was first demonstrated by Sirbuly *et al.* without delicate alignment of the two NWs (Fig. 6a-i and ii).[134] Optical routing in a rectangular grid of passive waveguides was also successfully demonstrated. The study proved the feasibility of intra-chip optical data communication in a platform composed of only the NW waveguides. Recently, a NW light emitter and detector were integrated on-chip through a micro-waveguide.[143,147] Core/shell InGaN/GaN with five radial quantum wells was exploited for the emitter and detector to reduce carrier transit time and circumvent the non-radiative recombination on the surface defects.[144–146] The emitter and detector were connected by a SiN waveguide fabricated by

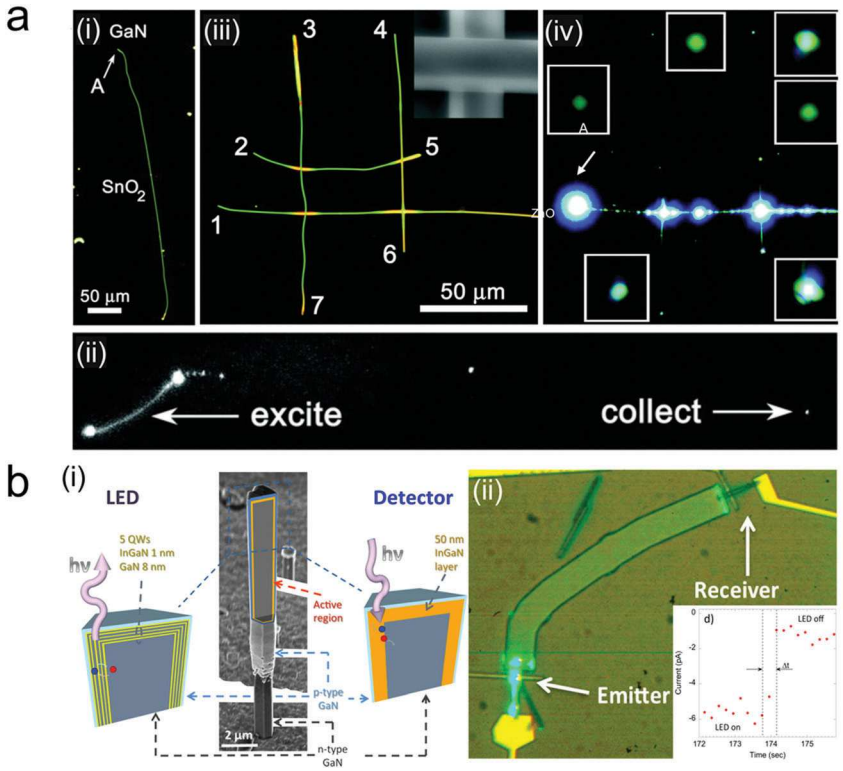

Fig. 6 Integrated optical communication platform for intrachip data communication consisting of a light emitter, passive waveguide, and photodetectors. Dark-field images of parallelly (a-i) and perpendicularly (a-iii) connected optical routing and the corresponding optical images of PL from the NWs as the input channels are pumped (a-iii and a-iv). Adapted with permission from ref. 134. Copyright 2005 National Academy of Sciences, USA. (b-i) SEM image and schematic of the internal structure for the NW LED and photodetector. (b-ii) Optical microscopy images of the integrated NW LED and photodetector under excitation of the LED. The inset shows the current variation speed between laser-on and off states. Adapted with permission from ref. 147. Copyright 2014 American Chemical Society.

nanolithography. However, the on–off transient is extraordinarily slow (<0.5 s) even with the core/shell heterostructure. Either inefficient injection of charge carriers or optical coupling among the waveguides might have caused the slow switching time. Further improvement of on–off transition time is enforced to take full advantage of optical waveguides over the copper-based electrical circuit.

4.2. Optical sensors

Optical sensors have a variety of advantages over the conventional electrical sensors in terms of sensitivity, response time, immunity to electromagnetic interference, and multiple routes for the detection of the change of the surrounding materials.[136] For optoelectronics, the tight mode confinement in NW waveguides is imperative. For the optical sensor, however, the vulnerability of the guided modes to the changes in the external environment is important for high sensitivity. Therefore, it is preferred to have a larger fraction of evanescence fields traveling outside of the NW waveguide.[136,148,149] SiO_2 nanowires physically drawn from an optical fiber are the most popular material choice for dielectric waveguide-based optical sensing, because of their simple and well-developed fabrication and surface modification methods,[136] and their uniform diameters and smooth surfaces. In addition, this fabrication method offers loss-free light input and output through the optical fiber, both ends of which can be easily connected to light sources and detectors.[148,150]

In the early stage, sensing the materials surrounding the NW has been demonstrated by measuring the change of output intensity.[151] The mechanism is straightforward, and it requires only a photodiode. Later, a variation of phase,[152] polarization, wavelength or transit time of light in the NW waveguide has been used to obtain more information about the surrounding materials.[136,153] However, they are extremely sensitive to other influences such as stress induced by the NW and temperature variation during measurement.[154,155] Above all, extreme difficulty in sensing or identifying specific molecules in a complex medium limited their applicability in labs and industry. To address this issue, markers such as dyes or quantum dots (QDs) sensitive to a specific molecule with a huge variation of absorbance or wavelength started to be used for sensing a target molecule regardless of the complexity of the media.[156]

In 2012, the author reported NW based single cell endoscopy which can shuttle light in and out of a single living cell without cell membrane damage or significant perturbation of the normal cellular process, facilitated by the small cross-section of the NW waveguide[157] (Fig. 7a). The NW endoscope was fabricated by integrating a SnO_2 NW with a tapered optical fiber to achieve efficient light coupling from the optical fiber to the NW. Light-activated spot cargo delivery with high spatiotemporal

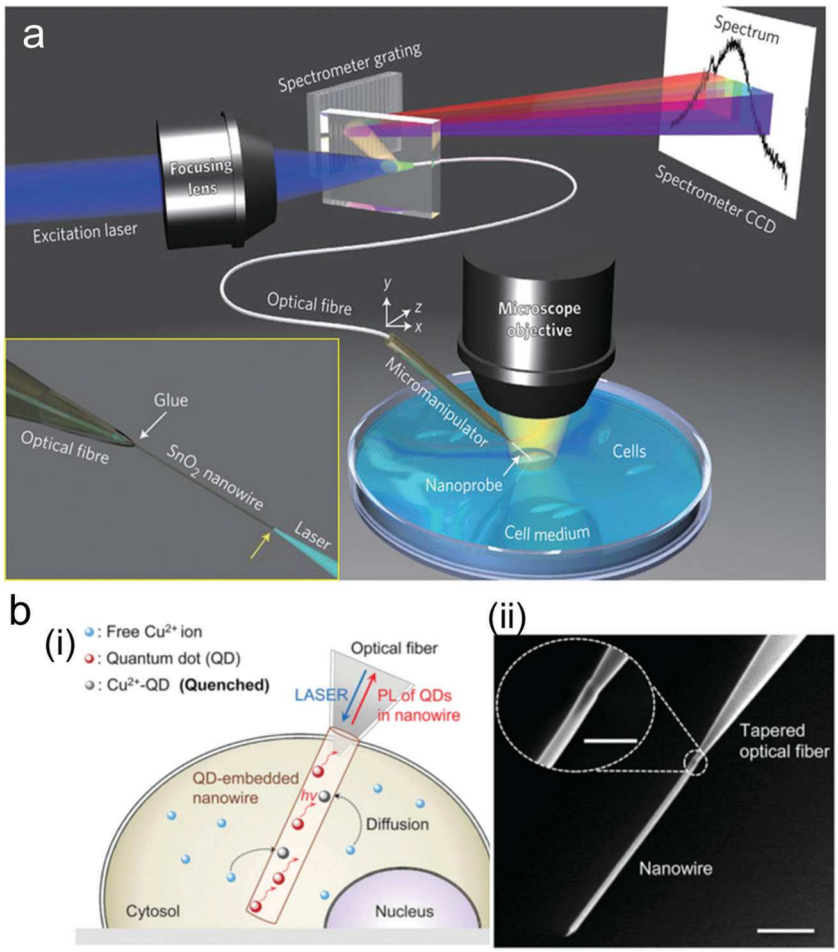

Fig. 7 Nanowire-based single-cell endoscopy probe. (a) Schematic illustration of a nanowire-based optical probe for single cell endoscopy. The inset shows schematic illustration of coupling light from an optical fiber to a SnO_2 nanowire. Adapted with permission from ref. 157. Copyright 2011 Springer Nature. (b) Schematic illustration (i) and SEM images (ii) of the nanowire endoscopy probe for quantitative sensing of Cu^{2+} ions in a living cell. Adapted with permission from ref. 159. Copyright 2016 John Wiley and Sons.

resolution and spot chemical sensing was demonstrated. Since then, several NW waveguides have been introduced for subcellular chemical detection.[158] In 2016, J. Lee *et al.* quantitatively measured Cu^{2+} ions specifically in single living cells using a QD embedded polymer NW[159] (Fig. 7b). A unique property of the endoscopy probe was that the photoluminescence signal was collected through the same light path used for light excitation. This signal collection configuration simplifies the device design, since complex optical components to focus or collect light with careful optical alignment are not required.

5. Application of plasmonic NW waveguides

While dielectric NW waveguides have a wide variety of material choices, material choices for plasmonic NW waveguides for the visible-NIR spectrum range have been limited mostly to Group 11 transition metals (Ag, Au and Cu) to maintain a reasonable propagation loss. Unlike Au and Cu, which have d-band transitions in the visible range that contribute to absorption losses, Ag is free of specific absorption in the entire visible and NIR spectral range. This has made Ag the most widely used material for NW waveguides where high performance and low loss are required. However, Ag tarnishes easily under ambient conditions. Therefore, Au, being chemically more stable, is also used at the expense of slightly increased propagation loss. It is worth noting that AgNWs synthesized by the polyol methods have a unique advantage over lithographically defined structures, not only because of their high crystallinity and smooth surface that guarantee the lowest loss possible, but also because these AgNWs have a thin layer of PVP molecules, a souvenir of the synthesis, absorbed on their surface to block environmental oxidants. So, the life-span of chemically synthesized AgNWs is considerably longer in the range of one to several days in air, making them the best choice of material for deep-subwavelength plasmonic waveguides within the vis-NIR range.

As discussed earlier in Section a, the major limitation of plasmonic waveguides compared to their dielectric counterparts is their high propagation loss, mainly due to ohmic loss. Similar to the dielectric waveguide, the plasmonic waveguide can support several modes and the number of modes increases

Table 2 Reported propagation lengths of Ag and Au nanowires

Material	Diameter (nm)	Wavelength (nm)	Substrate	Propagation length	Ref.
Ag	100	532	Air	6.2 μm[a]	3
		650		11.3 μm[a]	
		980		20.2 μm[a]	
	~100	830	Glass	3 ± 1 μm[b]	169
		628	Sol–gels	9.1 μm[b]	170
	110 ± 15	785	Glass	10.1 ± 0.4 μm[c]	161
	90–170	760–860	PMMA	11–17.5 μm[d]	162
	50–200	532	Glass	6 μm[d]	163
		650		11 μm[d]	
	260	532	Glass	6.77 μm[a]	164
		633		10.56 μm[a]	
		980		13.27 μm[a]	
	150–461	532	Air	150 nm: 7.3 μm (TM_0), 87.1 (HE_1)[a]	165
				280 nm: 12.7 μm (TM_0), 40.5 μm (HE_1)[a]	
				458 nm: 13.0 μm (TM_0), 24.4 μm (HE_1)[a]	
		658		150 nm: 17.5 μm (TM_0), no exist (HE_1)[a]	
				280 nm: 28.2 μm (TM_0), 159.1 μm (HE_1)[a]	
				461 nm: 40.4 μm (TM_0), 69.0 μm (HE_1)[a]	
	750	785	Glass	10.6 μm[a]	166
Au	60–100	760–860	PMMA	2.4–3.6 μm[d]	162
	210	980	Glass	5.6 μm[a]	167
		785		4.9 μm	
		650		3.4 μm[a]	
	~400	532	Glass	1.8 ± 0.4 μm[d]	168
	390 ± 60	785	Glass	3.5 μm[d]	171
	600 ± 220	800	Glass	12.3 ± 4.1 μm[e]	172
	380 ± 140				

[a] Tapered fiber. [b] Sidewall scattering. [c] Fabry–Perot resonator modes. [d] Fluorescence. [e] Scanning transient absorption microscopy.

as its diameter increases. In the case of AgNWs, two lowest order modes can be supported and simultaneously excited in the diameter range of 100–400 nm.[160] Each mode has a different propagation length, which is the figure of merit in describing the propagation loss and is defined by the length at which the intensity of the guided mode decays to $1/e$ or roughly 27%.[3] The weight of the two SPP modes in a Ag NW relies on the excitation technique, incident light wavelength and polarization, nanowire size and dielectric environment (substrate). As a result, propagation lengths reported for AgNWs are vastly different in the literature (Table 2). The influence of the weight of the modes is not limited to the overall propagation loss. Selective excitation of the mode in metal NWs is critical for many applications. For example, in near-field imaging with a AgNW as the optical probe (details in Section 5.3), tight localization of strong electromagnetic fields at the tip of the NW is required for high spatial resolution. In such a case, the lowest order mode with the highest momentum needs to be predominantly excited. On the other hand, the higher order mode is favorable in optical sensing (details in Section 5.2), since it has a larger skin depth, or in other words, its evanescent field penetrates deeper into the surroundings allowing for stronger interaction with the medium, which is important for boosting sensitivity. It has been shown that the selective excitation SPP modes can be achieved by changing the incident polarization.[173] However, to rationally tailor the excitation and propagation conditions in a AgNW towards a specific application, there must be a method to distinguish or decouple the SPP modes and estimate, at least roughly, the weight of the two modes. We have made the first step towards this goal by developing a mode interference method to successfully decouple the two modes on a free-standing AgNW, analyzed the propagation lengths of each, and their dependence on NW diameters and excitation wavelengths (Fig. 8).[165] Here, the tapered optical fiber was brought into contact with the free standing AgNW on the edge of a polydimethylsiloxane (PDMS) block and the intensity at the tip of the NW was measured while the probe was slid along the NW (Fig. 8a). The intense oscillation is a result of the beating or interference between the two modes, from which propagation parameters of each mode can be separately derived. Fig. 8b and c show the effective mode indices and propagation lengths calculated using the beating period of the two modes. A strong dependence on nanowire diameter was observed for both the propagation lengths and the weight of the supported SPP modes. Selective excitation of each mode can be achieved by choosing the correct diameter.

5.1. Optoelectronics: passive waveguides with deep-subwavelength confinement

In a plasmonic waveguide, a favorable mode for the passive waveguide is controversial due to its unique optical properties. The lowest order mode (TM_0) has an advantage over higher modes because it is less sensitive to the environment, easy to modulate (symmetric radiation at the end), and has a lower bending radius. On the other hand, the second lowest order mode (HE_1) has a longer propagation length and higher coupling efficiency with directional mode coupling due to a longer skin depth. Therefore, a selective excitation mode depending on the

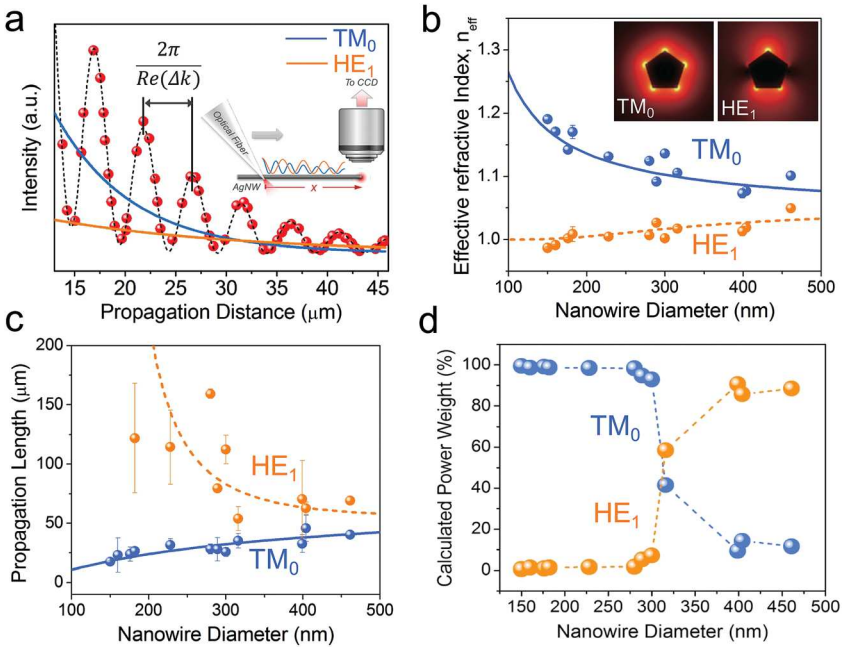

Fig. 8 Two lowest order SPP modes in a AgNW. (a) Measured emission intensity at the tip of the AgNW *versus* propagation distance. Inset: Schematic illustration of the emission intensity measurement. Attenuation curves of the TM_0 and HE_1 modes (blue and orange lines respectively) are deconvoluted from the experimental data. The wavelength of the incident light is 658 nm. Numerically and experimentally obtained effective refractive indices (b) and propagation lengths (c) of two SPP modes in the AgNW under 658 nm excitation. Insets: Electric field ($|E|$) distribution of the two modes in the AgNW. (d) Relative weight of two lowest order modes as a function of NW diameter under 658 nm excitation. Adapted with permission from ref. 165. Copyright 2017 Springer Nature.

application of the waveguide is carefully considered. Bending loss is also inevitable in the plasmonic NW waveguide. Wang *et al.* demonstrated a significant bending loss with a silver NW (Fig. 9a and b).[166] The results showed that the bending radius at which the loss starts to increase rapidly is even larger than that of the dielectric waveguide with a high refractive index difference. In the experiment, a long wavelength and thick NW was used which eventually affects the bending loss significantly in the following three ways. The long wavelength of excitation light firstly results in a lower wavevector (momentum) of SPPs. This wavevector is proportional to the coupling strength between the excitation light and surface charge oscillation. The higher the wavevector, the finer the confinement of the modes on the surface of the metal. Since light with long wavelengths was used in the experiment, the SPPs are not tightly bound to the surface of the metal and, as a result, a large fraction of the evanescence fields lose their binding to the metal surface and scatter at the bending part of the waveguide. Secondly, a thick NW can support higher order modes whose coupling strength is weaker than that of the lower order mode as can be seen in Fig. 8a. Fig. 9d and e compare the bending loss of two lowest order SPP modes in the AgNW waveguide. The lowest order mode (TM_0) with a high wavevector guided through the AgNW has a lower energy leakage from the bending part than the higher order mode (HE_1). Finally, the coupling strength of even the lowest order mode (TM_0) decreases as the diameter increases as shown in Fig. 8f and g. Almost all energy leaks from the bending part of the waveguide to free space with a thicker NW diameter. In conclusion, bending loss can be reduced by tightly confining light with surface charge oscillation. However, it finally brings about a large ohmic loss. Balancing of bending loss and Ohmic loss must be considered carefully before designing optical circuits. In addition, the weight of each mode should be fully understood which varies depending on the excitation methods and conditions.

5.2. Optical sensing

Compared with the dielectric waveguide, the plasmonic NW has distinct advantages in the field of optical sensing. First, in the plasmonic NW, energy propagates at the interface between the metal and the surrounding dielectric environment and it has a stronger evanescent field than its dielectric counterpart. Consequently, it has a higher sensitivity to changes in the environment. More importantly, the electromagnetic field is massively enhanced, giving rise to the possibility of incorporating Surface Enhanced Raman Spectroscopy (SERS) into the sensing mechanism. SERS is a powerful technique that enables the detection of low concentration molecules adsorbed on metal surfaces using amplified electric magnetic fields due to the localized SPPs. With a plasmonic nanogap, SERS has demonstrated a single-molecule detection capability.[174] In addition, each molecule has a unique Raman fingerprint, so that labelling is no longer a necessity to achieve molecular specificity, and allows qualitative, and even quantitative, chemical measurement in a native, untampered environment. This is especially important in cell biology to avoid tedious and complicated labelling

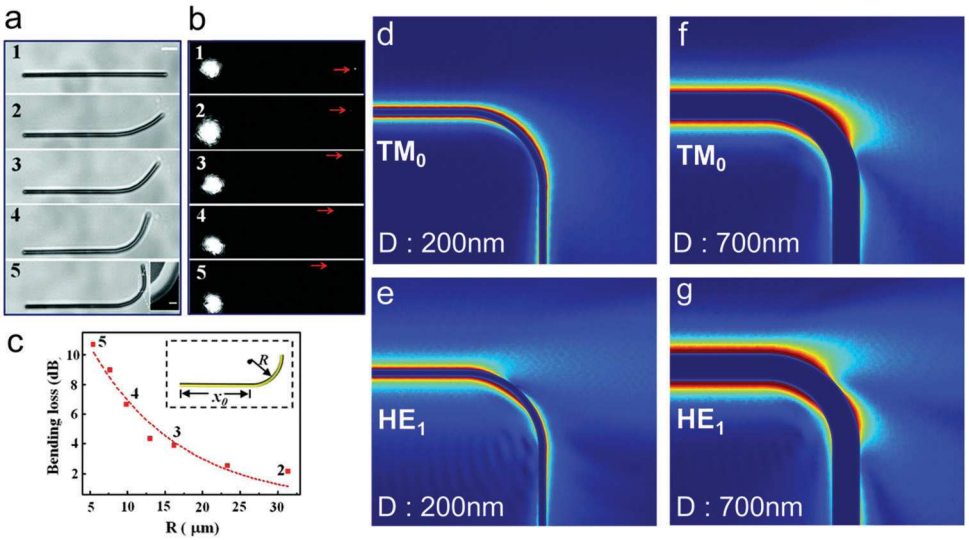

Fig. 9 Dependency of bending loss on bending radius, wavelength of excitation light, and NW diameter. (a) Bright-field optical images of a AgNW with different bending radii. The diameter and length of the AgNW are 750 nm and 45 μm respectively. The bending radii of the AgNW are 32, 16, 9, and 5 μm, respectively. The inset shows the SEM image of the curved section. (b) Dark-field optical images with different bending radii. A 758 nm laser is focused at the left end of the AgNW and the intensity of emitted light indicated by the red arrows was measured to obtain the bending loss. (c) Calculated bending loss as a function of bending radius after subtracting the propagation loss from the measured values of the emitted light intensity in (b). Adapted with permission from ref. 166. Copyright 2011 American Chemical Society. Electric field ($|E|$) distribution of propagating TM_0 (d) and HE_1 (e) SPP modes in a AgNW with 200 nm diameter. Electric field ($|E|$) distribution of TM_0 (f) and HE_1 (g) SPP modes in a AgNW with 700 nm diameter. The bending radius and wavelength for (d–g) are 1 μm and 700 nm respectively.

procedures, which can introduce unknown changes into cellular structures and functions. In 2014, G. Lu *et al.* measured Raman signals from a single living cell using a plasmonic NW waveguide mounted on a tungsten tip controlled by a micromanipulator (Fig. 10a).[175] In this work, the SPPs in the Ag NW were excited by focusing the excitation laser on a nanoparticle attached to the middle of the NW to minimize the background Raman signal from free-space excitation. The remote excitation SERS shows a clear Raman signature of biomolecules (*e.g.* proteins and lipids) in the cell due to the efficient optical excitation and the strong field enhancement at the nanoscale curvature of the metal tip. This is the first demonstration of using a plasmonic NW waveguide for intracellular chemical detection; however, more work needs to be done beyond proof-of-principle demonstrations and molecular specificity needs to be achieved for the practical application of plasmonic SERS endoscopes in chemical and biochemical sensing.

5.3. Near field imaging

Tip-enhanced Raman spectroscopy (TERS) is a powerful technique that combines the high chemical sensitivity of SERS and the high spatial resolution of scanning probe microscopies for nanoscale chemical imaging.[176,177] It has the illumination laser-focused on the apex of a metal STM probe or a metal-coated AFM probe, which confines and enhances the electromagnetic (EM) field through the excitation of localized surface plasmon resonances. Such a confinement not only increases the spatial resolution to the nanometer level,[178,179] but also compensates for the intrinsically small cross-sections of Raman processes.[180,181] Recently, T. Fujita *et al.* reported a TERS probe based on a plasmonic NW waveguide.[182] In this work, a silver NW was attached to a sharpened tungsten tip to form a TERS probe. For guidance of light through the silver NW, gold nanoparticles were integrated into the middle of the NW and used as the light coupling point. Compared to direct excitation wherein excitation light is focused at the tip of the NW, the remote excitation configuration demonstrated lower background noises. Although TERS scanning has not yet been demonstrated, this is an important step towards the application of the AgNW waveguide towards low-background near-field imaging.

6. Plasmonic–photonic hybrid NW waveguides

From the discussion of photonic and plasmonic NW waveguides in the previous two sections, one can inevitably see that despite the world-wide efforts and the massive progress in each field, the spells they are each under – the diffraction limit for photonic and the high ohmic loss for plasmonic NWs – were never lifted. Therefore, it is hard to rely on either of them alone to meet the ultimate requirements for integrated optoelectronics: deep-subwavelength, high-bandwidth, low loss and energy consumption. Over the last decade, more and more efforts have been devoted to combining plasmonic and photonic components into hybrid devices to get the best of both worlds. The first concept people experimented with is to couple plasmonic and photonic devices into a hybrid system. The idea is to use photonic NWs where high-efficiency is

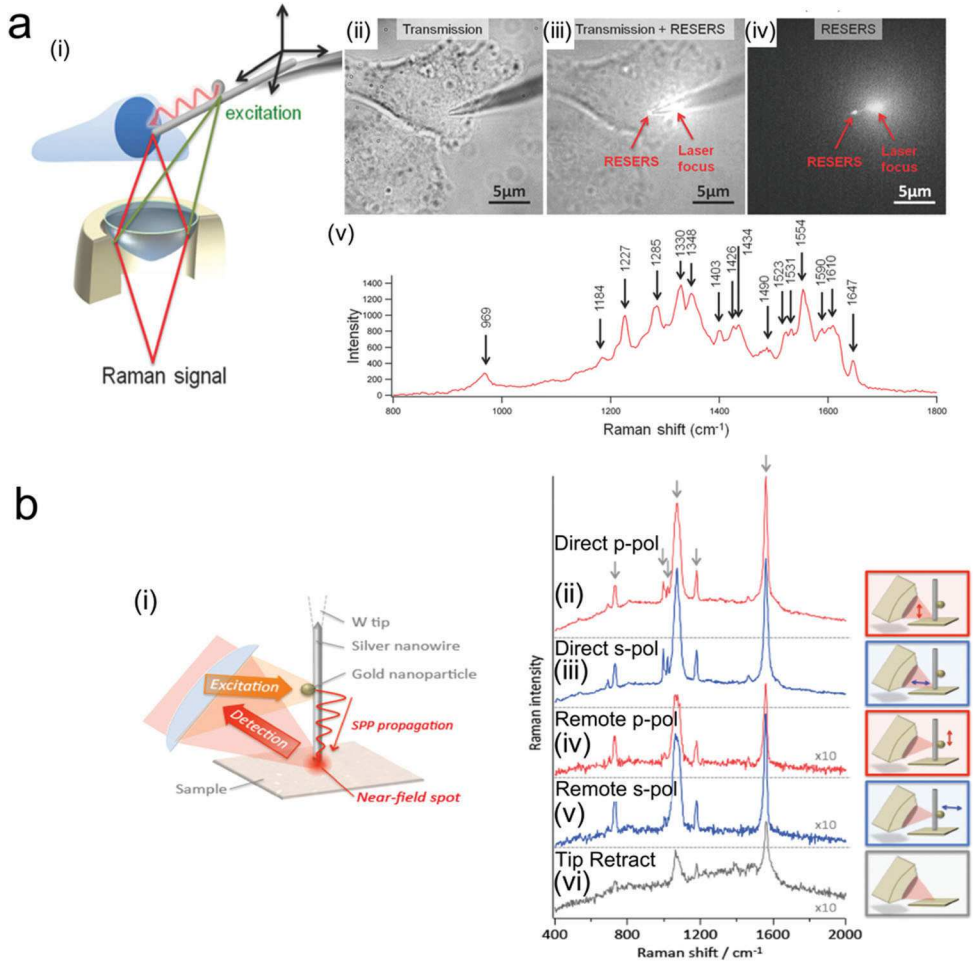

Fig. 10 Near field chemical sensing and imaging. (a-i) Schematic illustration of a remotely excited plasmonic nanowire SERS probe using a silver nanoparticle-attached silver nanowire. Image of optical transmission (a-ii), remote excitation of SERS under optical transmission (a-iii), and remote excitation of SERS only in a single living HeLa cell (a-iv). (a-v) Remotely excited SERS spectrum from nucleus of the living cell. Adapted with permission from ref. 175. Copyright 2014 John Wiley and Sons. (b-i) Schematic illustration of a AgNW TERS probe remotely excited using a gold nanoparticle. Raman spectrum of benzenethiol-modified Au with different excitations when the excitation laser is directly focused at the tip with p (b-ii) and s polarization (b-iii), when the laser is remotely focused at the gold nanoparticle with p (b-vi) and s polarization (b-v), and when the laser is focused on the substrate without the AgNW tip (vi). Adapted with permission from ref. 182. Copyright 2016 The Japan Society of Applied Physics.

required, *e.g.* emission, detection and optical interconnects on a chip-to-chip level and use plasmonic waveguides where tighter mode confinement or a high integration level is required. The two types of devices should be optically coupled to shuttle signals between each other.[3,183] The first design of dielectric–metallic–dielectric routing was demonstrated by the author in 2009 (Fig. 11a) to achieve optical coupling between two SnO_2 nanoribbon waveguides with a Ag nanowire plasmonic waveguide. The study conceptually demonstrated the possibility of using the dielectric NW for the optical bus and the metallic NW as an intra-chip optical path. At the same time, a ground-breaking new concept of the photonic–plasmonic hybrid on a single-NW level was proposed by Oulton *et al.*[184] It was shown by numerical simulation that the propagation lengths in a ''hybrid plasmonic waveguide'' can be increased to up to a few hundred micrometres. The proposed structure consists of a high-index semiconductor NW and a Ag film separated by a low-index dielectric spacer that is only several nanometres thick. The simulation results showed a strong confinement of electromagnetic energy in the 5 nm SiO_2 spacer, which provides a nearly loss-less channel for light propagation, leading to a superior propagation length. This idea can be generalized into a ''high-index NW/low-index spacer/metal'' sandwich model, which by an appropriate design can achieve tight mode confinement in the nm-sized spacer. Since most of the energy travels outside of the lossy metal, such a tight spatial confinement is accompanied also by much lower propagation loss.

Since then, there have been an increasing number of numerical simulations to optimize the hybrid mode structure to obtain a promising balance between the field confinement and the propagation length.[189,190] However, the experimental demonstration of a hybrid NW waveguide that meets the loss requirement for practical optoelectronic applications is still challenging, probably due to the large surface roughness and poor crystallinity of the deposited metal film or strip.[185,191,192]

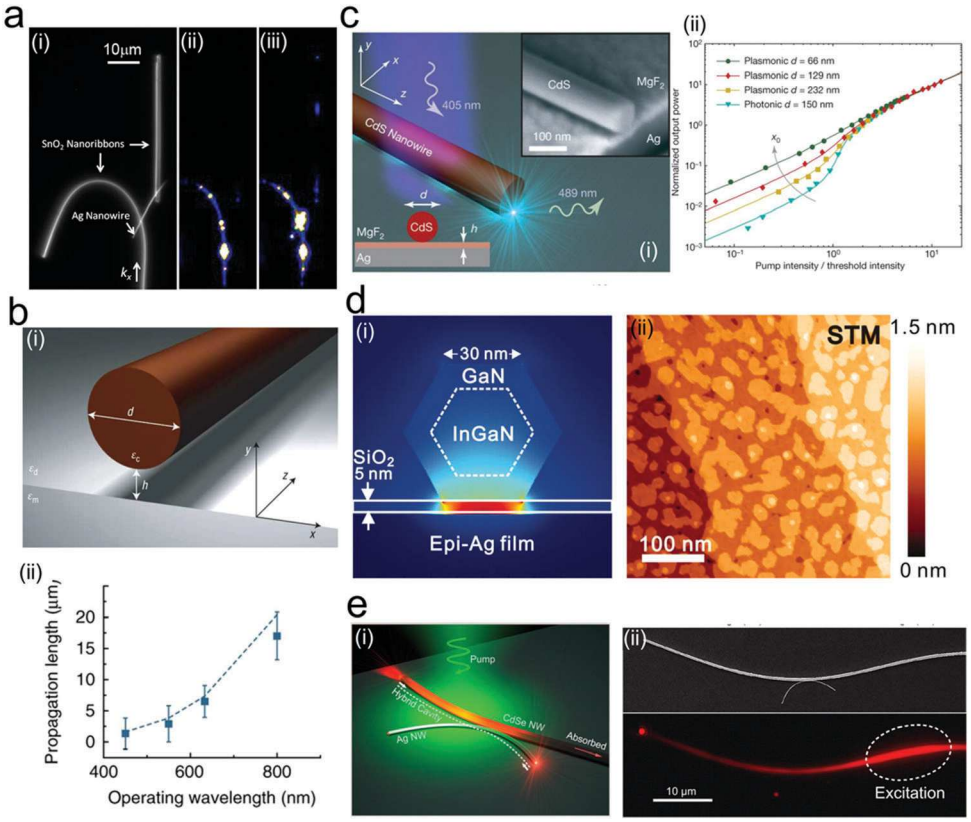

Fig. 11 Recent advances in hybrid waveguides. (a) Optical routing circuit between dielectric–metallic–dielectric waveguides. Adapted with permission from ref. 3. (b-i) Schematic of a dielectric cylindrical NW on a metal film with a dielectric gap. Adapted with permission from ref. 184. Copyright 2008 Springer Nature. (b-ii) Propagation length as a function of operating wavelength for ZnS/MgF_2/Ag hybrid plasmonic modes. Adapted with permission from ref. 185. Copyright 2011 Springer Nature. (c-i) Hybrid plasmonic laser consists of a CdS NW on a Ag film with a MgF_2 spacer. The top inset shows the SEM image of the plasmonic laser. (c-ii) Lasing threshold as a function of pump intensity for different CdS nanowire diameters. Adapted with permission from ref. 186. Copyright 2009 Springer Nature. (d-i) Energy density distribution of a single InGaN@GaN core–shell nanorod on an epitaxial Ag film with a 5 nm SiO_2 spacer. (d-ii) STM image of an epitaxial Ag film with 4 nm thickness. Adapted with permission from ref. 187. Copyright 2012 The American Association for the Advancement of Science. (e-i) Schematic of a hybrid photon–plasmon NW laser consisting of CdSe and AgNWs. (e-ii) SEM image and optical microscopy images of the lasing CdSe/AgNW hybrid photon plasmon NW. Adapted with permission from ref. 188. Copyright 2013 The American Chemical Society.

However, hybrid modes have found huge success in realizing the smallest lasers. The concept of a plasmonic laser has always been attractive due to the promise of nm-sized mode volume; however, the large ohmic loss of plasmonic NWs makes them poor cavities with quality factors in single digits. In a hybrid cavity, *e.g.*, CdS NW(gain)/MgF_2(spacer)/Ag, the lasing mode is tightly restricted to the nm-sized dielectric spacer between the NW and the Ag film, which greatly reduces the loss (Fig. 11c and d). Extremely strong mode confinement was demonstrated in the CdS NW/MgF_2/Ag hybrid laser[186] with six-fold enhancement of the spontaneous emission rate compared to the photonic laser (Fig. 11c). The optical fields in the hybrid laser rival the smallest commercial transistor gate sizes and reconcile the length scales of electronics and optics. Following this work, room-temperature lasing at different UV-Vis-NIR wavelengths has been realized in different hybrid nanowire lasers, and the reduction of mode volume and propagation loss using an atomically smooth metal film from epitaxial growth was demonstrated[187,193–196] (Fig. 11d). There have been considerable efforts to increase the temperature stability and reduce the lasing threshold by incorporating quantum elements into the hybrid plasmonic waveguide.[187,197] Although lasing at room temperature has not yet been demonstrated, the quantum dot-based hybrid plasmonic nanowire laser shows a significant improvement of temperature stability in the range of 7 to 125 K and remarkably low lasing threshold ($\sim$120 μJ cm^{-2} at 7 K) of the plasmonic modes highly confined near the metal–dielectric interface.[197] To take the full advantage of the enhanced Purcell and spontaneous emission coupling factors and realize room-temperature lasing, it will require delicate localization of the quantum dots in the dielectric waveguide and the optimization of the spacer between the nanowire and metal substrate. Lastly, we want to highlight a unique design of a nanowire laser with a longitudinal hybrid cavity and spatially separated photonic and plasmonic outputs.[188] By near-field coupling a high-gain CdSe NW and a 100 nm diameter Ag NW (Fig. 11e), stimulated emission was achieved at room-temperature with a plasmon mode area of $0.008\lambda^2$. Such a device may find unique applications in the high-efficiency coupling of single-photon emitters and ultra-sensitivity optical sensing.

7. Conclusion and outlook

The capability to confine, manipulate and transmit electromagnetic energy at the nanoscale is crucial for highly integrated and efficient nano-optical signal-processing and sensing devices and circuits. Chemically synthesized nanowires, due to their high crystallinity, low defect level, atomically smooth surfaces, and impressive tunability in size, structure and composition, represent an important class of building blocks for subwavelength signal propagation and processing. Here, we reviewed two classes of nanowire waveguides, photonic and plasmonic, discussed their distinctly different light propagation mechanisms and behaviours, and compared their strengths and limitations in the context of different subwavelength applications, and how they can work synergistically in hybrid devices to combine the advantages of the low energy loss and high optical gain in photonic materials and the tight energy confinement in plasmonic materials to achieve high-performance, deep-subwavelength devices that reconcile the length scales of electronics and optics.

We would also like to note that although remarkable device performances have been demonstrated in a wide range of photonic NWs for light emission, propagation and detection, further development of auxiliary components, such as the interconnector, coupler, splitter, polarizer, modulator, *etc.*, should accompany this. Equally urgent is the development of integration techniques between chemically synthesized NWs and electronic signal processors to take full advantage of the performance and versatility of nanowire waveguides. Alternatively, bottom-up assembly of independent all-optical systems from nanowire elements that assume various functions, such as power generation (nanowire solar cells), light generation, routing and detection, may be feasible, especially for nano-optical sensing.

A substantially large room still exists for optical sensing and imaging with NW waveguides. In particular, the exploitation of the strong evanescence fields in either dielectric or metallic waveguide in high-sensitivity, label-free chemical analysis is still in its infancy. The ability of plasmonic and hybrid waveguides to deliver and focus light into the nanoconfined region, combined with the strong local field enhancement can open up new and promising avenues for nano-resolution chemical and compositional imaging that has a huge impact on biological, material and catalysis research.

Conflicts of interest

There are no conflicts to declare.

References

1 M. Born and E. Wolf, Principles of Optics: Electromagnetic Theory of Propagation, *Interference and Diffraction of Light*, Cambridge University Press, Cambridge, 7th edn, 1999.
2 M. Law, D. J. Sirbuly, J. C. Johnson, J. Goldberger, R. J. Saykally and P. Yang, *Science*, 2004, **305**, 1269.
3 R. Yan, P. Pausauskie, J. Huang and P. Yang, *Proc. Natl. Acad. Sci. U. S. A.*, 2009, **106**, 21045–21050.
4 R. Yan, D. Gargas and P. Yang, *Nat. Photonics*, 2009, **3**, 569.
5 X. Guo, Y. Ma, Y. Wang and L. Tong, *Laser Photonics Rev.*, 2013, **7**, 855–881.
6 S. W. Eaton, M. Lai, N. A. Gibson, A. B. Wong, L. Dou, J. Ma, L.-W. Wang, S. R. Leone and P. Yang, *Proc. Natl. Acad. Sci. U. S. A.*, 2016, **113**, 1993–1998.
7 Y. Ma, X. Guo, X. Wu, L. Dai and L. Tong, *Adv. Opt. Photonics*, 2013, **5**, 216–273.
8 G. Lifante, *Integrated photonics: fundamentals*, Wiley Online Library, 2003.
9 S. A. Maier, *Plasmonics: fundamentals and applications*, Springer Science & Business Media, 2007.
10 D. Sarid and W. Challener, *Modern introduction to surface plasmons: theory, mathematica modeling, and applications*, Cambridge University Press, 2010.
11 N. P. Dasgupta, J. Sun, C. Liu, S. Brittman, S. C. Andrews, J. Lim, H. Gao, R. Yan and P. Yang, *Adv. Mater.*, 2014, **26**, 2137–2184.
12 M. I. Stockman, *Phys. Rev. Lett.*, 2004, **93**, 137404.
13 I. A. Larkin, M. I. Stockman, M. Achermann and V. I. Klimov, *Phys. Rev. B: Condens. Matter Mater. Phys.*, 2004, **69**, 121403.
14 J. Takahara, S. Yamagishi, H. Taki, A. Morimoto and T. Kobayashi, *Opt. Lett.*, 1997, **22**, 475–477.
15 A. Zhang, G. Zheng and C. M. Lieber, *Nanowires: Building blocks for nanoscience and nanotechnology*, Springer, 2016.
16 R. S. Wagner and W. C. Ellis, *Appl. Phys. Lett.*, 1964, **4**, 89–90.
17 A. M. Morales and C. M. Lieber, *Science*, 1998, **279**, 208–211.
18 Y. Wu and P. Yang, *Chem. Mater.*, 2000, **12**, 605–607.
19 M. Law, J. Goldberger and P. Yang, *Annu. Rev. Mater. Res.*, 2004, **34**, 83–122.
20 H.-J. Choi, *Semiconductor Nanostructures for Optoelectronic Devices*, Springer, 2012, pp. 1–36.
21 M. R. Ramdani, E. Gil, C. Leroux, Y. André, A. Trassoudaine, D. Castelluci, L. Bideux, G. Monier, C. Robert-Goumet and R. Kupka, *Nano Lett.*, 2010, **10**, 1836–1841.
22 E. Gil-Lafon, J. Napierala, D. Castelluci, A. Pimpinelli, R. Cadoret and B. Gérard, *J. Cryst. Growth*, 2001, **222**, 482–496.
23 G. Avit, K. Lekhal, Y. André, C. Bougerol, F. Réveret, J. Leymarie, E. Gil, G. Monier, D. Castelluci and A. Trassoudaine, *Nano Lett.*, 2014, **14**, 559–562.
24 Q. Gao, D. Saxena, F. Wang, L. Fu, S. Mokkapati, Y. Guo, L. Li, J. Wong-Leung, P. Caroff, H. H. Tan and C. Jagadish, *Nano Lett.*, 2014, **14**, 5206–5211.
25 Z. Yang, J. Xu, P. Wang, X. Zhuang, A. Pan and L. Tong, *Nano Lett.*, 2011, **11**, 5085–5089.
26 J. Tatebayashi, S. Kako, J. Ho, Y. Ota, S. Iwamoto and Y. Arakawa, *Nat. Photonics*, 2015, **9**, 501.
27 X. Ma, Y. Zhu, S. Kim, Q. Liu, P. Byrley, Y. Wei, J. Zhang, K. Jiang, S. Fan and R. Yan, *Nano Lett.*, 2016, **16**, 6896–6902.
28 F. Kim, K. Sohn, J. Wu and J. Huang, *J. Am. Chem. Soc.*, 2008, **130**, 14442–14443.

29 F. Qian, Y. Li, S. Gradečak, H.-G. Park, Y. Dong, Y. Ding, Z. L. Wang and C. M. Lieber, *Nat. Mater.*, 2008, **7**, 701.
30 Y. Wu, R. Fan and P. Yang, *Nano Lett.*, 2002, **2**, 83–86.
31 M. S. Gudiksen, L. J. Lauhon, J. Wang, D. C. Smith and C. M. Lieber, *Nature*, 2002, **415**, 617–620.
32 K. Tateno, G. Zhang, H. Gotoh and T. Sogawa, *Nano Lett.*, 2012, **12**, 2888–2893.
33 J. Tatebayashi, Y. Ota, S. Ishida, M. Nishioka, S. Iwamoto and Y. Arakawa, *Appl. Phys. Lett.*, 2012, **100**, 263101.
34 J. J. Glennon, R. Tang, W. E. Buhro and R. A. Loomis, *Nano Lett.*, 2007, **7**, 3290–3295.
35 L. Zhen, M. Xuedan, S. Qiao, W. Zhe, L. Jian, Z. Zhonghua, Q. S. Zhang, S. C. Smith, L. Gaoqing and M. Alf, *Eur. J. Inorg. Chem.*, 2010, 4325–4331.
36 W. Fudong and W. E. Buhro, *Small*, 2010, **6**, 573–581.
37 V. Protasenko, S. Gordeyev and M. Kuno, *J. Am. Chem. Soc.*, 2007, **129**, 13160–13171.
38 Y.-H. Liu, F. Wang, J. Hoy, V. L. Wayman, L. K. Steinberg, R. A. Loomis and W. E. Buhro, *J. Am. Chem. Soc.*, 2012, **134**, 18797–18803.
39 Y. Sun and Y. Xia, *Adv. Mater.*, 2002, **14**, 833–837.
40 Y. Sun, Y. Yin, B. T. Mayers, T. Herricks and Y. Xia, *Chem. Mater.*, 2002, **14**, 4736–4745.
41 G. Singh, A. T. J. van Helvoort, S. Bandyopadhyay, S. Volden, J.-P. Andreassen and W. R. Glomm, *Appl. Surf. Sci.*, 2014, **311**, 780–788.
42 K. Vasilev, T. Zhu, M. Wilms, G. Gillies, I. Lieberwirth, S. Mittler, W. Knoll and M. Kreiter, *Langmuir*, 2005, **21**, 12399–12403.
43 N. Pazos-Pérez, D. Baranov, S. Irsen, M. Hilgendorff, L. M. Liz-Marzán and M. Giersig, *Langmuir*, 2008, **24**, 9855–9860.
44 Z. Huo, C.-k. Tsung, W. Huang, X. Zhang and P. Yang, *Nano Lett.*, 2008, **8**, 2041–2044.
45 M. H. Huang, S. Mao, H. Feick, H. Yan, Y. Wu, H. Kind, E. Weber, R. Russo and P. Yang, *Science*, 2001, **292**, 1897–1899.
46 Y. Gao, H. Cansizoglu, K. G. Polat, S. Ghandiparsi, A. Kaya, H. H. Mamtaz, A. S. Mayet, Y. Wang, X. Zhang, T. Yamada, E. P. Devine, A. F. Elrefaie, S.-Y. Wang and M. S. Islam, *Nat. Photonics*, 2017, **11**, 301.
47 M. L. Calvo and V. Lakshminarayanan, *Optical Waveguides: From Theory to Applied Technologies*, CRC Press, 2007.
48 B. Chen, T. Sun, X. Qiao, X. Fan and F. Wang, *Adv. Opt. Mater.*, 2015, **3**, 1577–1581.
49 W. Xu, T. K. Lee, B.-S. Moon, D. Zhou, H. Song, Y.-J. Kim, S. K. Kwak, P. Chen and D.-H. Kim, *Nanoscale*, 2017, **9**, 9238–9245.
50 Y. Wang, L. Zhang, C. Liang, G. Wang and X. Peng, *Chem. Phys. Lett.*, 2002, **357**, 314–318.
51 X. Fang, T. Zhai, U. K. Gautam, L. Li, L. Wu, Y. Bando and D. Golberg, *Prog. Mater. Sci.*, 2011, **56**, 175–287.
52 C. Jin, K. Zhu, G. Peterson, Z. Zhang, Z. Jian, Y. Wei and D. Zheng, *Solid State Commun.*, 2018, **269**, 1–5.
53 G. Yue, P. Yan, D. Yan, X. Fan, M. Wang, D. Qu and J. Liu, *Appl. Phys. A: Mater. Sci. Process.*, 2006, **84**, 409–412.
54 X.-J. Xu, G.-T. Fei, W.-H. Yu, X.-W. Wang, L. Chen and L.-D. Zhang, *Nanotechnology*, 2005, **17**, 426.
55 M. Chang, X. L. Cao, X.-J. Xu and L. Zhang, *Phys. Lett. A*, 2008, **372**, 273–276.
56 M. S. Park, G. X. Wang, Y. M. Kang, D. Wexler, S. X. Dou and H. K. Liu, *Angew. Chem.*, 2007, **119**, 764–767.
57 S. Sun, G. Meng, Y. Wang, T. Gao, M. Zhang, Y. Tian, X. Peng and L. Zhang, *Appl. Phys. A: Mater. Sci. Process.*, 2003, **76**, 287–289.
58 Z. W. Pan, Z. R. Dai and Z. L. Wang, *Science*, 2001, **291**, 1947–1949.
59 O. Lupan, L. Chow, G. Chai, A. Schulte, S. Park and H. Heinrich, *Mater. Sci. Eng., B*, 2009, **157**, 101–104.
60 A. Zhang, G. Zheng and C. M. Lieber, *Nanowires*, Springer, 2016.
61 K. Saron and M. Hashim, *Superlattices Microstruct.*, 2013, **56**, 55–63.
62 T. Kuykendall, P. Pauzauskie, S. Lee, Y. Zhang, J. Goldberger and P. Yang, *Nano Lett.*, 2003, **3**, 1063–1066.
63 X. Wang, C. J. Summers and Z. L. Wang, *Nano Lett.*, 2004, **4**, 423–426.
64 Y. Kong, D. Yu, B. Zhang, W. Fang and S. Feng, *Appl. Phys. Lett.*, 2001, **78**, 407–409.
65 C. Ternon, G. Rey, M. Labeau, N. Thiré, C. Jimenez, L. Rapenne and D. Bellet, *ECS Trans.*, 2009, **25**, 437–443.
66 L. E. Greene, M. Law, J. Goldberger, F. Kim, J. C. Johnson, Y. Zhang, R. J. Saykally and P. Yang, *Angew. Chem., Int. Ed.*, 2003, **42**, 3031–3034.
67 M. Zheng, L. Zhang, G. Li and W. Shen, *Chem. Phys. Lett.*, 2002, **363**, 123–128.
68 S. E. Ahn, J. S. Lee, H. Kim, S. Kim, B. H. Kang, K. H. Kim and G. T. Kim, *Appl. Phys. Lett.*, 2004, **84**, 5022–5024.
69 F. Zhuge, T. Yanagida, K. Nagashima, H. Yoshida, M. Kanai, B. Xu, A. Klamchuen, G. Meng, Y. He and S. Rahong, *J. Phys. Chem. C*, 2012, **116**, 24367–24372.
70 J.-M. Wu, W.-T. Wu and H. C. Shih, *J. Electrochem. Soc.*, 2005, **152**, G613–G616.
71 I. S. Cho, Z. Chen, A. J. Forman, D. R. Kim, P. M. Rao, T. F. Jaramillo and X. Zheng, *Nano Lett.*, 2011, **11**, 4978–4984.
72 X. Zhang, B. Yao, L. Zhao, C. Liang, L. Zhang and Y. Mao, *J. Electrochem. Soc.*, 2001, **148**, G398–G400.
73 R. Sui, A. S. Rizkalla and P. A. Charpentier, *J. Phys. Chem. B*, 2006, **110**, 16212–16218.
74 B. Xiang, H. Zhang, G. Li, F. Yang, F. Su, R. Wang, J. Xu, G. Lu, X. Sun and Q. Zhao, *Appl. Phys. Lett.*, 2003, **82**, 3330–3332.
75 X. Zhang, K. Ip, Z. Liu, Y. Leung, Q. Li and S. Hark, *Appl. Phys. Lett.*, 2004, **84**, 2641–2643.
76 A. Dong, F. Wang, T. L. Daulton and W. E. Buhro, *Nano Lett.*, 2007, **7**, 1308–1313.
77 L. Li, Y. Yang, X. Huang, G. Li and L. Zhang, *J. Phys. Chem. B*, 2005, **109**, 12394–12398.
78 C. Ye, G. Meng, Y. Wang, Z. Jiang and L. Zhang, *J. Phys. Chem. B*, 2002, **106**, 10338–10341.
79 X. Wu and Y. Tao, *J. Cryst. Growth*, 2002, **242**, 309–312.

80 T. Zhai, X. Fang, Y. Bando, Q. Liao, X. Xu, H. Zeng, Y. Ma, J. Yao and D. Golberg, *ACS Nano*, 2009, **3**, 949–959.
81 J. Sun and W. E. Buhro, *Angew. Chem.*, 2008, **120**, 3259–3262.
82 D. Routkevitch, T. Bigioni, M. Moskovits and J. M. Xu, *J. Phys. Chem.*, 1996, **100**, 14037–14047.
83 E. Janik, J. Sadowski, P. Dłużewski, S. Kret, L. Baczewski, A. Petroutchik, E. Łusakowska, J. Wrobel, W. Zaleszczyk and G. Karczewski, *Appl. Phys. Lett.*, 2006, **89**, 133114.
84 F. Wang, A. Dong, J. Sun, R. Tang, H. Yu and W. E. Buhro, *Inorg. Chem.*, 2006, **45**, 7511–7521.
85 J. Zhang, S. Jin, H. C. Fry, S. Peng, E. Shevchenko, G. P. Wiederrecht and T. Rajh, *J. Am. Chem. Soc.*, 2011, **133**, 15324–15327.
86 D. Xu, X. Shi, G. Guo, L. Gui and Y. Tang, *J. Phys. Chem. B*, 2000, **104**, 5061–5063.
87 S. Neretina, R. A. Hughes, J. Britten, N. Sochinskii, J. Preston and P. Mascher, *Nanotechnology*, 2007, **18**, 275301.
88 V. Di Carlo, P. Prete, V. G. Dubrovskii, Y. Berdnikov and N. Lovergine, *Nano Lett.*, 2017, **17**, 4075–4082.
89 A. Zhao, G. Meng, L. Zhang, T. Gao, S. Sun and Y. Pang, *Appl. Phys. A: Mater. Sci. Process.*, 2003, **76**, 537–539.
90 T. Ma, M. Guo, M. Zhang, Y. Zhang and X. Wang, *Nanotechnology*, 2007, **18**, 035605.
91 M. C. Kum, B. Y. Yoo, Y. W. Rheem, K. N. Bozhilov, W. Chen, A. Mulchandani and N. V. Myung, *Nanotechnology*, 2008, **19**, 325711.
92 J. Motohisa, J. Noborisaka, J. Takeda, M. Inari and T. Fukui, *J. Cryst. Growth*, 2004, **272**, 180–185.
93 Y. Wu and P. Yang, *J. Am. Chem. Soc.*, 2001, **123**, 3165–3166.
94 C.-Y. Wen, M. Reuter, J. Tersoff, E. Stach and F. Ross, *Nano Lett.*, 2009, **10**, 514–519.
95 A. T. Heitsch, D. D. Fanfair, H.-Y. Tuan and B. A. Korgel, *J. Am. Chem. Soc.*, 2008, **130**, 5436–5437.
96 J. Mallet, M. Molinari, F. Martineau, F. Delavoie, P. Fricoteaux and M. Troyon, *Nano Lett.*, 2008, **8**, 3468–3474.
97 Z.-x. Yang, N. Han, M. Fang, H. Lin, H.-Y. Cheung, S. Yip, E.-J. Wang, T. Hung, C.-Y. Wong and J. C. Ho, *Nat. Commun.*, 2014, **5**, 5249.
98 Z.-x. Yang, L. Liu, S. Yip, D. Li, L. Shen, Z. Zhou, N. Han, T. F. Hung, E. Y.-B. Pun and X. Wu, *ACS Nano*, 2017, **11**, 4237–4246.
99 M. Jeppsson, K. A. Dick, H. A. Nilsson, N. Sköld, J. B. Wagner, P. Caroff and L.-E. Wernersson, *J. Cryst. Growth*, 2008, **310**, 5119–5122.
100 J. C. Johnson, H.-J. Choi, K. P. Knutsen, R. D. Schaller, P. Yang and R. J. Saykally, *Nat. Mater.*, 2002, **1**, 106.
101 J. A. Zapien, Y. Jiang, X. M. Meng, W. Chen, F. C. K. Au, Y. Lifshitz and S. T. Lee, *Appl. Phys. Lett.*, 2004, **84**, 1189–1191.
102 X. Duan, Y. Huang, R. Agarwal and C. M. Lieber, *Nature*, 2003, **421**, 241–245.
103 A. H. Chin, S. Vaddiraju, A. V. Maslov, C. Z. Ning, M. K. Sunkara and M. Meyyappan, *Appl. Phys. Lett.*, 2006, **88**, 163115.
104 X. Wang, M. Shoaib, X. Wang, X. Zhang, M. He, Z. Luo, W. Zheng, H. Li, T. Yang and X. Zhu, *ACS Nano*, 2018, **12**, 6170–6178.
105 M. A. Zimmler, J. Bao, F. Capasso, S. Müller and C. Ronning, *Appl. Phys. Lett.*, 2008, **93**, 051101.
106 S. A. Dayeh, A. F. i Morral and C. Jagadish, *Semiconductor Nanowires II: Properties and Applications*, Academic Press, 2016.
107 S. Wang, Z. Hu, H. Yu, W. Fang, M. Qiu and L. Tong, *Opt. Express*, 2009, **17**, 10881–10886.
108 B. E. Saleh and M. C. Teich, *Fundamentals of photonics*, 2007.
109 H. Gao, A. Fu, S. C. Andrews and P. Yang, *Proc. Natl. Acad. Sci. U. S. A.*, 2013, **110**, 865–869.
110 Y. Xiao, C. Meng, P. Wang, Y. Ye, H. Yu, S. Wang, F. Gu, L. Dai and L. Tong, *Nano Lett.*, 2011, **11**, 1122–1126.
111 S. W. Eaton, A. Fu, A. B. Wong, C.-Z. Ning and P. Yang, *Nat. Rev. Mater.*, 2016, **1**, 16028.
112 P. Guo, X. Zhuang, J. Xu, Q. Zhang, W. Hu, X. Zhu, X. Wang, Q. Wan, P. He, H. Zhou and A. Pan, *Nano Lett.*, 2013, **13**, 1251–1256.
113 Y. Fu, H. Zhu, C. C. Stoumpos, Q. Ding, J. Wang, M. G. Kanatzidis, X. Zhu and S. Jin, *ACS Nano*, 2016, **10**, 7963–7972.
114 W. Lu and C. M. Lieber, *J. Phys. D: Appl. Phys.*, 2006, **39**, R387.
115 C. J. Barrelet, A. B. Greytak and C. M. Lieber, *Nano Lett.*, 2004, **4**, 1981–1985.
116 F. Qian, S. Gradecak, Y. Li, C.-Y. Wen and C. M. Lieber, *Nano Lett.*, 2005, **5**, 2287–2291.
117 E. Garnett and P. Yang, *Nano Lett.*, 2010, **10**, 1082–1087.
118 L. K. Yeh, K. Y. Lai, G. J. Lin, P. H. Fu, H. C. Chang, C. A. Lin and H. He Jr, *Adv. Energy Mater.*, 2011, **1**, 506–510.
119 T. J. Kempa, J. F. Cahoon, S.-K. Kim, R. W. Day, D. C. Bell, H.-G. Park and C. M. Lieber, *Proc. Natl. Acad. Sci. U. S. A.*, 2012, **109**, 1407–1412.
120 L. Cao, J. S. White, J.-S. Park, J. A. Schuller, B. M. Clemens and M. L. Brongersma, *Nat. Mater.*, 2009, **8**, 643–647.
121 H. Kind, H. Yan, B. Messer, M. Law and P. Yang, *Adv. Mater.*, 2002, **14**, 158–160.
122 J. Wang, M. S. Gudiksen, X. Duan, Y. Cui and C. M. Lieber, *Science*, 2001, **293**, 1455–1457.
123 Y. Gu, E.-S. Kwak, J. L. Lensch, J. E. Allen, T. W. Odom and L. J. Lauhon, *Appl. Phys. Lett.*, 2005, **87**, 043111.
124 Y. Dan, K. Seo, K. Takei, J. H. Meza, A. Javey and K. B. Crozier, *Nano Lett.*, 2011, **11**, 2527–2532.
125 J. Tang, Z. Huo, S. Brittman, H. Gao and P. Yang, *Nat. Nanotechnol.*, 2011, **6**, 568.
126 M. A. Kinch, *Fundamentals of infrared detector materials*, SPIE Press, Bellingham, 2007.
127 J. Miao, W. Hu, N. Guo, Z. Lu, X. Zou, L. Liao, S. Shi, P. Chen, Z. Fan and J. C. Ho, *ACS Nano*, 2014, **8**, 3628–3635.
128 R. LaPierre, M. Robson, K. Azizur-Rahman and P. Kuyanov, *J. Phys. D: Appl. Phys.*, 2017, **50**, 123001.
129 Z. Li, X. Yuan, L. Fu, K. Peng, F. Wang, X. Fu, P. Caroff, T. P. White, H. H. Tan and C. Jagadish, *Nanotechnology*, 2015, **26**, 445202.

130 L. Ma, W. Hu, Q. Zhang, P. Ren, X. Zhuang, H. Zhou, J. Xu, H. Li, Z. Shan and X. Wang, *Nano Lett.*, 2014, **14**, 694–698.
131 L. Rigutti, M. Tchernycheva, A. D. L. Bugallo, G. Jacopin, F. Julien, L. F. Zagonel, K. March, O. Stephan, M. Kociak and R. Songmuang, *Nano Lett.*, 2010, **10**, 2939–2943.
132 W. Deng, L. Huang, X. Xu, X. Zhang, X. Jin, S.-T. Lee and J. Jie, *Nano Lett.*, 2017, **17**, 2482–2489.
133 X. Dai, S. Zhang, Z. Wang, G. Adamo, H. Liu, Y. Huang, C. Couteau and C. Soci, *Nano Lett.*, 2014, **14**, 2688–2693.
134 D. J. Sirbuly, M. Law, P. Pauzauskie, H. Yan, A. V. Maslov, K. Knutsen, C.-Z. Ning, R. J. Saykally and P. Yang, *Proc. Natl. Acad. Sci. U. S. A.*, 2005, **102**, 7800–7805.
135 X. C. Tong, *Advanced materials for integrated optical waveguides*, Springer, 2016.
136 X. Guo, Y. Ying and L. Tong, *Acc. Chem. Res.*, 2013, **47**, 656–666.
137 H. Yu, S. Wang, J. Fu, M. Qiu, Y. Li, F. Gu and L. Tong, *Appl. Opt.*, 2009, **48**, 4365–4369.
138 Y. A. Vlasov and S. J. McNab, *Opt. Express*, 2004, **12**, 1622–1631.
139 A. Gondarenko, J. S. Levy and M. Lipson, *Opt. Express*, 2009, **17**, 11366–11370.
140 J. F. Bauters, M. J. Heck, D. D. John, J. S. Barton, C. M. Bruinink, A. Leinse, R. G. Heideman, D. J. Blumenthal and J. E. Bowers, *Opt. Express*, 2011, **19**, 24090–24101.
141 T. Horikawa, D. Shimura and T. Mogami, *MRS Commun.*, 2016, **6**, 9–15.
142 F. Li, S. D. Jackson, C. Grillet, E. Magi, D. Hudson, S. J. Madden, Y. Moghe, C. O'Brien, A. Read and S. G. Duvall, *Opt. Express*, 2011, **19**, 15212–15220.
143 M. D. Brubaker, P. T. Blanchard, J. B. Schlager, A. W. Sanders, A. Roshko, S. M. Duff, J. M. Gray, V. M. Bright, N. A. Sanford and K. A. Bertness, *Nano Lett.*, 2013, **13**, 374–377.
144 A. Higuera-Rodriguez, B. Romeira, S. Birindelli, L. Black, E. Smalbrugge, P. Van Veldhoven, W. Kessels, M. Smit and A. Fiore, *Nano Lett.*, 2017, **17**, 2627–2633.
145 S. Boubanga-Tombet, J. B. Wright, P. Lu, M. R. Williams, C. Li, G. T. Wang and R. P. Prasankumar, *ACS Photonics*, 2016, **3**, 2237–2242.
146 W. Liu, C. Mounir, G. Rossbach, T. Schimpke, A. Avramescu, H.-J. Lugauer, M. Strassburg, U. Schwarz, B. Deveaud and G. Jacopin, *Appl. Phys. Lett.*, 2018, **112**, 052106.
147 M. Tchernycheva, A. Messanvi, A. de Luna Bugallo, G. Jacopin, P. Lavenus, L. Rigutti, H. Zhang, Y. Halioua, F. Julien and J. Eymery, *Nano Lett.*, 2014, **14**, 3515–3520.
148 G. Brambilla, *J. Opt.*, 2010, **12**, 043001.
149 F. Gu, L. Zhang, X. Yin and L. Tong, *Nano Lett.*, 2008, **8**, 2757–2761.
150 L. Tong, R. R. Gattass, J. B. Ashcom, S. He, J. Lou, M. Shen, I. Maxwell and E. Mazur, *Nature*, 2003, **426**, 816–819.
151 F. Warken, E. Vetsch, D. Meschede, M. Sokolowski and A. Rauschenbeutel, *Opt. Express*, 2007, **15**, 11952–11958.
152 J. Lou, L. Tong and Z. Ye, *Opt. Express*, 2005, **13**, 2135–2140.
153 G. Y. Chen, M. Ding, T. P. Newson and G. Brambilla, *Open Opt. J.*, 2013, **7**, 32–57.
154 L. Zhang, J. Lou and L. Tong, *Photonic Sens.*, 2011, **1**, 31–42.
155 B. Lee, *Opt. Fiber Technol.*, 2003, **9**, 57–79.
156 D. J. Sirbuly, A. Tao, M. Law, R. Fan and P. Yang, *Adv. Mater.*, 2007, **19**, 61–66.
157 R. Yan, J.-H. Park, Y. Choi, C.-J. Heo, S.-M. Yang, L. P. Lee and P. Yang, *Nat. Nanotechnol.*, 2012, **7**, 191–196.
158 G. Shambat, S.-R. Kothapalli, J. Provine, T. Sarmiento, J. Harris, S. S. Gambhir and J. Vučković, *Nano Lett.*, 2013, 13, 4999–5005.
159 J. Lee, H. R. Lee, J. Pyo, Y. Jung, J. Y. Seo, H. G. Ryu, K. T. Kim and J. H. Je, *Adv. Mater.*, 2016, **28**, 4071–4076.
160 S. Zhang, H. Wei, K. Bao, U. Håkanson, N. J. Halas, P. Nordlander and H. Xu, *Phys. Rev. Lett.*, 2011, **107**, 096801.
161 H. Ditlbacher, A. Hohenau, D. Wagner, U. Kreibig, M. Rogers, F. Hofer, F. R. Aussenegg and J. R. Krenn, *Phys. Rev. Lett.*, 2005, **95**, 257403.
162 B. Wild, L. Cao, Y. Sun, B. P. Khanal, E. R. Zubarev, S. K. Gray, N. F. Scherer and M. Pelton, *ACS Nano*, 2012, **6**, 472–482.
163 T. Shegai, Y. Huang, H. Xu and M. Käll, *Appl. Phys. Lett.*, 2010, **96**, 103114.
164 Y. Ma, X. Li, H. Yu, L. Tong, Y. Gu and Q. Gong, *Opt. Lett.*, 2010, **35**, 1160–1162.
165 S. Kim, S. Bailey, M. Liu and R. Yan, *Nano Res.*, 2017, **10**, 2395–2404.
166 W. Wang, Q. Yang, F. Fan, H. Xu and Z. L. Wang, *Nano Lett.*, 2011, **11**, 1603–1608.
167 X. Li, X. Guo, D. Wang and L. Tong, *Opt. Commun.*, 2014, **323**, 119–122.
168 D. Solis Jr, W.-S. Chang, B. P. Khanal, K. Bao, P. Nordlander, E. R. Zubarev and S. Link, *Nano Lett.*, 2010, **10**, 3482–3485.
169 A. W. Sanders, D. A. Routenberg, B. J. Wiley, Y. Xia, E. R. Dufresne and M. A. Reed, *Nano Lett.*, 2006, **6**, 1822–1826.
170 A. L. Pyayt, B. Wiley, Y. Xia, A. Chen and L. Dalton, *Nat. Nanotechnol.*, 2008, **3**, 660–665.
171 S. Nauert, A. Paul, Y.-R. Zhen, D. Solis Jr, L. Vigderman, W.-S. Chang, E. R. Zubarev, P. Nordlander and S. Link, *ACS Nano*, 2013, **8**, 572–580.
172 K. Yu, M. S. Devadas, T. A. Major, S. S. Lo and G. V. Hartland, *J. Phys. Chem. C*, 2014, **118**, 8603–8609.
173 Z. Li, K. Bao, Y. Fang, Y. Huang, P. Nordlander and H. Xu, *Nano Lett.*, 2010, **10**, 1831–1835.
174 K. Kneipp, Y. Wang, H. Kneipp, L. T. Perelman, I. Itzkan, R. R. Dasari and M. S. Feld, *Phys. Rev. Lett.*, 1997, **78**, 1667.
175 G. Lu, H. De Keersmaecker, L. Su, B. Kenens, S. Rocha, E. Fron, C. Chen, P. Van Dorpe, H. Mizuno and J. Hofkens, *Adv. Mater.*, 2014, **26**, 5124–5128.
176 N. Hayazawa, Y. Inouye, Z. Sekkat and S. Kawata, *Opt. Commun.*, 2000, **183**, 333–336.
177 R. M. Stockle, Y. D. Suh, V. Deckert and R. Zenobi, *Chem. Phys. Lett.*, 2000, **318**, 131–136.
178 R. Zhang, Y. Zhang, Z. C. Dong, S. Jiang, C. Zhang, L. G. Chen, L. Zhang, Y. Liao, J. Aizpurua, Y. Luo, J. L. Yang and J. G. Hou, *Nature*, 2013, **498**, 82–86.
179 C. Chen, N. Hayazawa and S. Kawata, *Nat. Commun.*, 2014, **5**, 3312.

180 M. D. Sonntag, J. M. Klingsporn, L. K. Garibay, J. M. Roberts, J. A. Dieringer, T. Seideman, K. A. Scheidt, L. Jensen, G. C. Schatz and R. P. V. Duyne, *J. Phys. Chem. C*, 2012, **116**, 478–483.
181 M. D. Sonntag, E. A. Pozzi, N. Jiang, M. C. Hersam and R. P. V. Duyne, *J. Phys. Chem. Lett.*, 2014, **5**, 3125–3130.
182 Y. Fujita, P. Walke, S. De Feyter and H. Uji, *Jpn. J. Appl. Phys.*, 2016, **55**, 08NB03.
183 X. Guo, M. Qiu, J. Bao, B. J. Wiley, Q. Yang, X. Zhang, Y. Ma, H. Yu and L. Tong, *Nano Lett.*, 2009, **9**, 4515–4519.
184 R. F. Oulton, V. J. Sorger, D. Genov, D. Pile and X. Zhang, *Nat. Photonics*, 2008, **2**, 496.
185 V. J. Sorger, Z. Ye, R. F. Oulton, Y. Wang, G. Bartal, X. Yin and X. Zhang, *Nat. Commun.*, 2011, **2**, 331.
186 R. F. Oulton, V. J. Sorger, T. Zentgraf, R.-M. Ma, C. Gladden, L. Dai, G. Bartal and X. Zhang, *Nature*, 2009, **461**, 629.
187 Y.-J. Lu, J. Kim, H.-Y. Chen, C. Wu, N. Dabidian, C. E. Sanders, C.-Y. Wang, M.-Y. Lu, B.-H. Li and X. Qiu, *Science*, 2012, **337**, 450–453.
188 X. Wu, Y. Xiao, C. Meng, X. Zhang, S. Yu, Y. Wang, C. Yang, X. Guo, C. Z. Ning and L. Tong, *Nano Lett.*, 2013, **13**, 5654–5659.
189 X. Y. He, Q. J. Wang and S. F. Yu, *Plasmonics*, 2012, **7**, 571–577.
190 Y. Bian, Z. Zheng, X. Zhao, J. Zhu and T. Zhou, *Opt. Express*, 2009, **17**, 21320–21325.
191 D. Y. Fedyanin, D. I. Yakubovsky, R. V. Kirtaev and V. S. Volkov, *Nano Lett.*, 2015, **16**, 362–366.
192 J. Tian, Z. Ma, Q. Li, Y. Song, Z. Liu, Q. Yang, C. Zha, J. Åkerman, L. Tong and M. Qiu, *Appl. Phys. Lett.*, 2010, **97**, 231121.
193 E. Bermúdez-Ureña, G. Tutuncuoglu, J. Cuerda, C. L. C. Smith, J. Bravo-Abad, S. I. Bozhevolnyi, A. Fontcuberta i Morral, F. J. García-Vidal and R. Quidant, *Nano Lett.*, 2017, **17**, 747–754.
194 T. P. H. Sidiropoulos, R. Röder, S. Geburt, O. Hess, S. A. Maier, C. Ronning and R. F. Oulton, *Nat. Phys.*, 2014, **10**, 870.
195 Y.-J. Lu, C.-Y. Wang, J. Kim, H.-Y. Chen, M.-Y. Lu, Y.-C. Chen, W.-H. Chang, L.-J. Chen, M. I. Stockman, C.-K. Shih and S. Gwo, *Nano Lett.*, 2014, **14**, 4381–4388.
196 Q. Zhang, G. Li, X. Liu, F. Qian, Y. Li, T. C. Sum, C. M. Lieber and Q. Xiong, *Nat. Commun.*, 2014, **5**, 4953.
197 J. Ho, J. Tatebayashi, S. Sergent, C. F. Fong, Y. Ota, S. Iwamoto and Y. Arakawa, *Nano Lett.*, 2016, **16**, 2845–2850.

